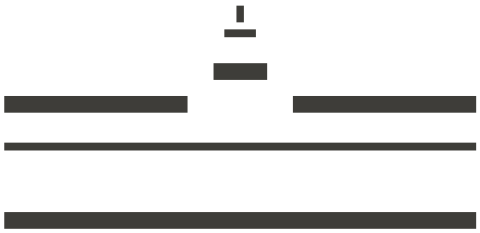

WWU

Investigations of background light sources in photomultiplier tubes operated at negative high voltage

Master Thesis

presented at Westfälische Wilhelms-Universität Münster
Institut für Kernphysik

by

Florian Trittmaack

Supervisor and first examiner: Prof. Dr. Alexander Kappes

Westfälische Wilhelms-Universität Münster

Second examiner: Prof. Dr. Christian Weinheimer

Westfälische Wilhelms-Universität Münster

February 2018

"Alles muss, nix kann."

Rocket Beans TV

Introduction

The universe has been fascinating humanity for thousands of years. At first only the constellations were admired and interpreted, then the planet pits were investigated and in recent years one has ventured more and more into the depths of the universe to unravel new secrets and solve cosmic mysteries. But now we get help on this journey from the neutrino discovered in 1930 by Wolfgang Pauli, the so-called ghost particle, which missed its discoverer shortly after its postulation. At that time he thought: these particles could never be discovered. "*I have done a terrible thing; I have postulated a particle that can not be detected*". However, it turned out that this neutrino was not a poltergeist but even very helpful in exploring the universe. With its almost negligible mass and electrical neutrality, the neutrino can travel long distances undisturbed and thus transmit information from hitherto unknown regions. Fortunately, Pauli was not right about his fears, as physicists have now managed to detect neutrinos and elicit information from them.

At the present time, there are many "ghost busters" who specialize in the various properties of neutrinos, such as mass or neutrino oscillation. But the greatest "ghost buster" of this time tries to catch the most energetic ghost particles: The IceCube Observatory. A Detector that extends over 1 km^3 deep in the ice of the South Pole. The IceCube Observatory was specifically designed to detect the highest-energy neutrinos and is still one of the most successful experiments of its kind. In order to deprive as many neutrinos as possible, IceCube is equipped with over 500 "eyes". These "eyes" are the digital optical modules. These DOMs consist of a 10 ten-inch photomultiplier. At the time of writing, the extension of the IceCube observatory is being planned to observe even more and higher energetic neutrinos, and new optical modules will be developed for this purpose.

The working group of Professor Kappes at the University of Münster deals with the development of these modules. In particular on the development of a new module which features 24 smaller PMTs in it. Understanding the used photomultipliers is an important task to understand the behavior of the whole module. The work presented in this thesis takes care of the dark rates of PMTs and the interaction of PMTs placed close together, so that nothing stands in the way of a new chapter in the endless journey through the mysteries in the universe.

Contents

Chapter 1

The building blocks of the universes

Most of the known world is built from two fermions and one lepton: the up and the down quark and the electron, but with a closer look it turns out that there are a lot more particles. The Standard Model of particle physics is a theory that connects all the up to now known elementary particles. There are four different classes of particles, which are shown in figure 1.0.1. In the following, these classes will be introduced. Beginning with the quarks (blue in the figure) containing six listed types in the standard model, all mesons and baryons are built by two or three quarks. For example, the up and down quarks are the constituents of the proton and the neutron. The other four quarks or anti-quarks, the charm and strange quark and the top and bottom quark, do not appear in the world we deal with every day.

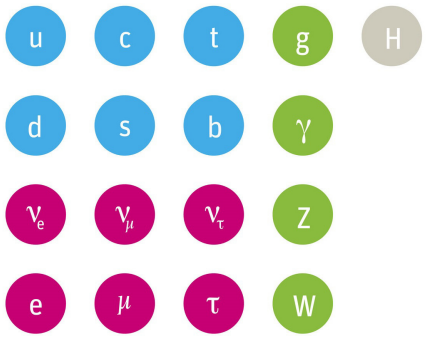

Figure 1.0.1: A sketch of the standard model with all elementary particles that form matter containing quarks, leptons, gauge bosons and the Higgs boson.

Electrons are also part of the fermions but in the lepton group (purple). The two additional leptons with their corresponding neutrinos ν are muons and tauons. Electrons have a mass of 511 keV, a muon is ca 200 times heavier (105.6 MeV) and the tau is the heaviest of these three with 1777 MeV [1]. The three neutrinos are massless[1] according to the Standard Model and have a very low interaction cross-section. Neutrinos take a crucial part in this thesis and are presented in more detail in chapter 1.2.

The second class in the standard model are the gauge bosons (green) which correspond to three of the four fundamental forces: electromagnetic (photon, γ), weak nuclear force ($W^{\pm}$ and Z^0-Boson) and the strong nuclear force (gluon, g). The fourth force of gravitation has no known boson in the Standard Model yet. The last class (gray) are the scalar bosons, has only one member: the Higgs boson. The Higgs, discovered in 2012 is responsible for the mass of the gauge bosons [3].

Particles introduced in this chapter are often found in the universe, some of them have very high energies and are called cosmic rays. The next chapters provide a closer look at cosmic rays and the production mechanism.

1.1 Cosmic rays, the bombardment of information

Cosmic rays are bombarding the earth all around the clock. Since 1912 cosmic rays are known and first detected by V. F. Hess. Today, the composition of particles in cosmic rays which are all charged particles is well known. Protons are with 90 % the most prominent

[1] Since 1987 it is proven by the neutrinos oscillation that at least two neutrinos do have a mass [2].

part of the cosmic rays, the rest are 9 % alpha nuclei [4] and the leftover 1 % consists of heavier nuclei like iron and also of electrons, positrons and anti-protons. In figure 1.1.1 the flux of the cosmic rays against the broad energy spectrum. . The all-particle flux

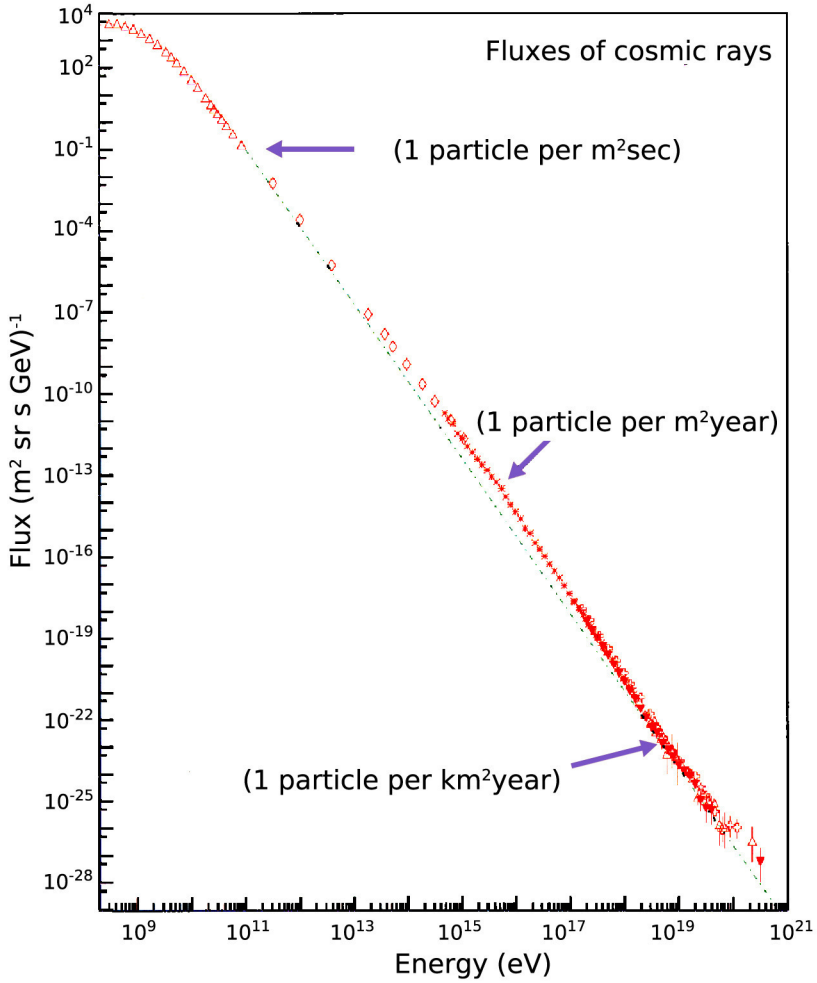

Figure 1.1.1: The flux of the cosmic ray is plotted against energy spectrum of the cosmic rays, with the “knee” and the “ankle”.

follows a simple broken power-law

$$\frac{dN}{dE} \propto E^{-n}, \tag{1.1.1}$$

in the general case the exponent has a value of $n \approx 2.7$ but in the region between 10^{15} eV to 10^{16} eV is changes to $n \approx 3$. This stays like that until energies of $10^{18.5}$ eV where the exponent goes back to $n \approx 2.7$. The first changing point in n is called the “knee” [5, 6]. The cosmic rays before the “knee” are assumed to come from a galactic supernova, where

the rays after the “knee” are more likely to originate in other more energetic galactic sources. The location of the second switch of the exponent is called the “ankle”, from that energy on the origins of the cosmic rays are believed to be extragalactic. Energies from this range up to the maximum are the most interesting range for the cosmic ray astronomy and the search for the origins of the cosmic rays, which are yet not developed. There are a few promising candidates to take in account, like Active Galactic Nuclei (AGN), pulsars, micro-quasars or Gamma Ray Bursts (GRB) (more information about this can be found in [7].

As presented before the main component of the cosmic rays are charged particles like protons and electrons but also neutral particles are generated while the acceleration process. The charged particles are easy to detect but to reconstruct the path of these particles does not lead to the right localization of their origins. Because of the electromagnetic fields which crisscross the universe, they are deflected, this problem is sketched in figure 1.1.2.

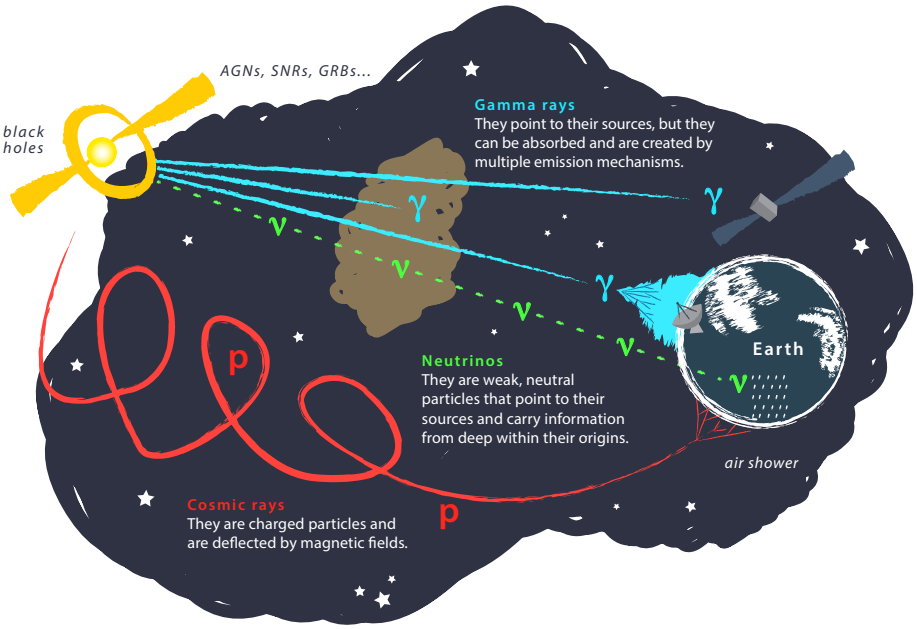

Figure 1.1.2: A sketch for the different ways particles take in the universe. Electrons and protons are deflected by the electromagnetic field, photons are absorbed on their way and neutrinos can reach the earth [8].

In fact, charged particles are detected on the earth eg. by the Pierre Auger Observatory and these experiments are able to distinguish the energy and to track back their incoming direction. So photons would be an obvious choice to search for the sources mentioned before, they are neutral and by now it is rather easy to detect with air Cerenkov detectors

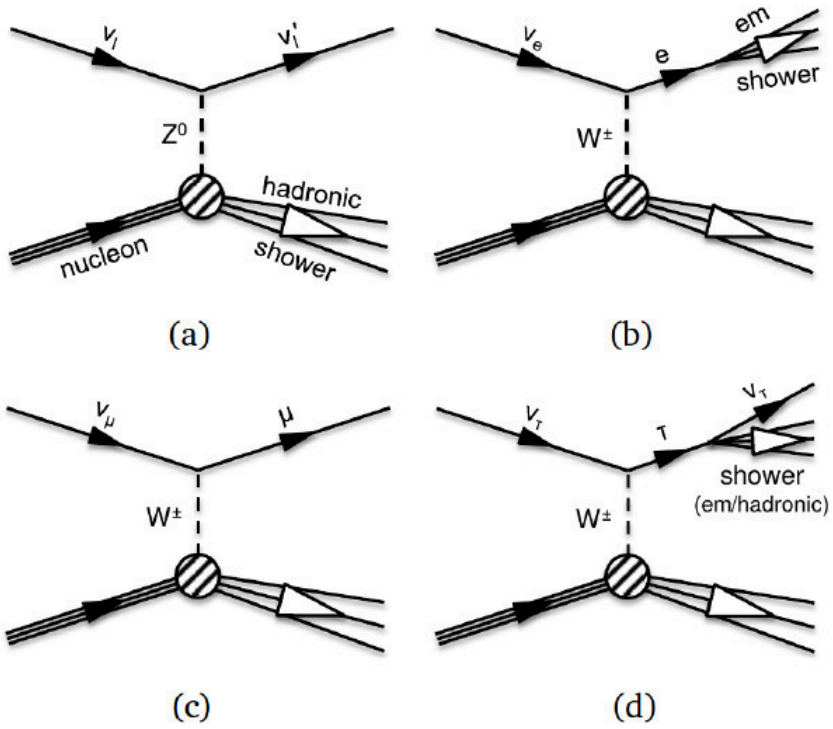

Figure 1.1.3: The Feynman diagrams of the four interaction channels [8].

like the Hess telescope [9] and we also get all in formations from them like the direction and energy. Nevertheless, photons with too high energies have a high probability to be absorbed or scatter in interstellar media, or even interact with the photon background noise. Also, photons can be produced by leptonic and hadronic acceleration [10] while only hadronic sources are interesting.

For these reasons only neutrinos are left to find the sources, they are neural and due to the tiny interaction cross section, the probability to scatter or being absorbed by matter in the universe is very low. This brings us to the next problem: How can we measure neutral charged, nearly massless and rarely interacting particles, which are only interacting gravitationally or weakly? To counter the poor interaction probability we need a large detector volume. The detection by the gravitational force can be neglected as the weakest of all forces and the negligible mass of the neutrinos. So the weak force is left over to detect the neutrinos. The weak force has three different gauge bosons: the electrical charged W^+- and W^- boson and the neutral charged Z^0-boson. That means neutrinos are able to weakly interact via charged current (CC) and neutral current interactions (NC) with nuclei and leptons.

The main interaction channel for the neutrinos at energies in the range of GeV to several PeV is the deep inelastic scattering with nucleons. The possible neutral and

charged current interactions are:

$$\nu_l + N \rightarrow \nu_l + X \text{ (NC)}, \ \nu_l + N \rightarrow l + X \ (CC) \tag{1.1.2}$$

Where ν_l is the neutrino or antineutrino with its flavor l, N represents the nucleus, so either a proton or a neutron. The l in the charged current is a lepton which corresponds to the neutrino flavor and X stands for several hadronic particles. With this knowledge, the foundation to detect neutrinos was built since we are not able to measure neutrinos directly it is only possible to detect the secondary leptons or hadronic showers of the mentioned reactions. Figure 1.1.3 shows the are four main interactions as Feynman diagrams.

So neutrinos are the main channel for the searches of the sources of cosmic rays the next chapter will provide a detailed look on neutrinos.

1.2 Neutrinos, the messenger particles

In 1930 Wolfgang Pauli postulated neutrinos to solve the problem of the continuous spectrum of the beta minus decay [11]. The neutrino was the missing third participant which abducted some energy and left behind a contentious spectrum for the electron energy. That particle had to be very light and neutrally charged. In 1956 the neutrino was detected by Clyde L. Cowan and Frederick Reines in a nuclear power station. In 2015 the noble price was given to Takaaki Kajita and Arthur B. McDonald for the discovery of neutrino oscillation in 1988. In this thesis, the neutrino oscillation will not be explained in detail, only the fact that due to the oscillation it is known that neutrinos have to be massive (more information can be found in [2]).The mass of the neutrino not developed yet but physicists from the KATRIN collaboration are working on the measurement for the upper limit down to 0.2 eV of the mass of the $\overline{\nu}_{e^-}$ in Karlsruhe [12].

The spectrum of the neutrino energy is very broad and it is important to know how and with which energy cosmic neutrinos were produced and how many of them are there, so which flux do they have. In figure 1.2.1 the neutrino flux is plotted against their energy. It is clearly noticeable that neutrinos with low energy are more frequently than high energetic neutrinos. The greatest flux of neutrinos are cosmological neutrinos with the lowest energy. The nucleosynthesis in the sun and supernovae, old and young, are responsible for a high flux with low energetic neutrinos.

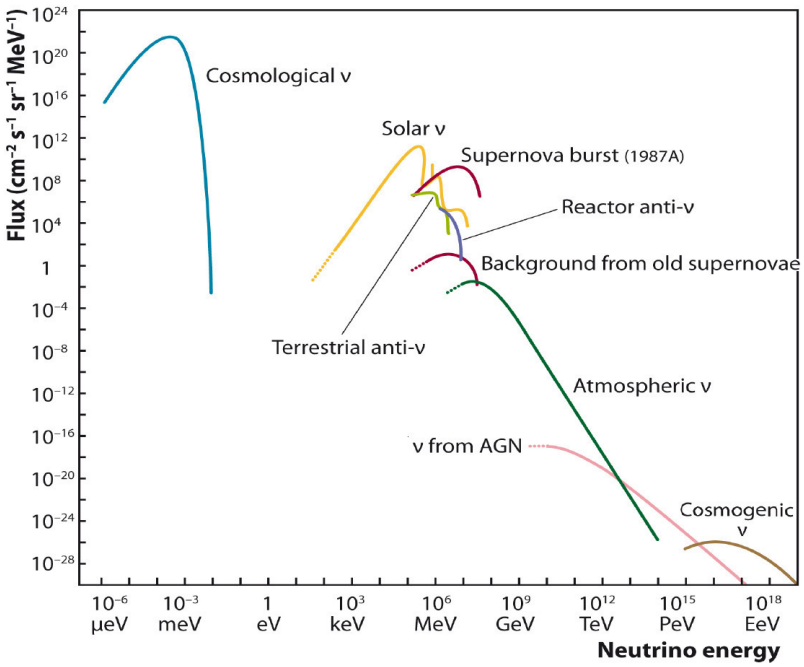

Figure 1.2.1: The energy spectrum of neutrinos plotted against the flux for different neutrinos source, e.g. the sun, supernovae, and AGNs [5].

The rest of this spectrum can roughly be sorted in three different categories of neutrinos by their origin: atmospheric neutrinos, GZK-neutrinos, and cosmic neutrinos These are the neutrinos with the highest energy and are candidates to find the cosmic ray sources.

Atmospheric neutrinos are, like the name suggests, produced in the atmosphere of the earth and the energy is in the range of GeV. When a high energetic particle of the cosmic rays hits an air molecule it will generate a so-called air shower, a cascade of hadronic and leptonic particles. These particles are produced by strong, electromagnetic or weak interaction mechanisms, depending on the initial particle, and its surrounding parameters. The energy of the initial particle will be distributed between the generated particles in each step of the cascade. The end result of such an air shower are up to millions produced particles, which are mostly exotic and with a short lifetime. An example is displayed in figure 1.2.2. Air showers are an often used to measure the cosmic rays in form of photons and electrons, which are two of the end results of the cascade, a famous example for an air shower detector is the Pierre Auger Observatory.
The main channels of the neutrino production in air showers are the decay of pions:

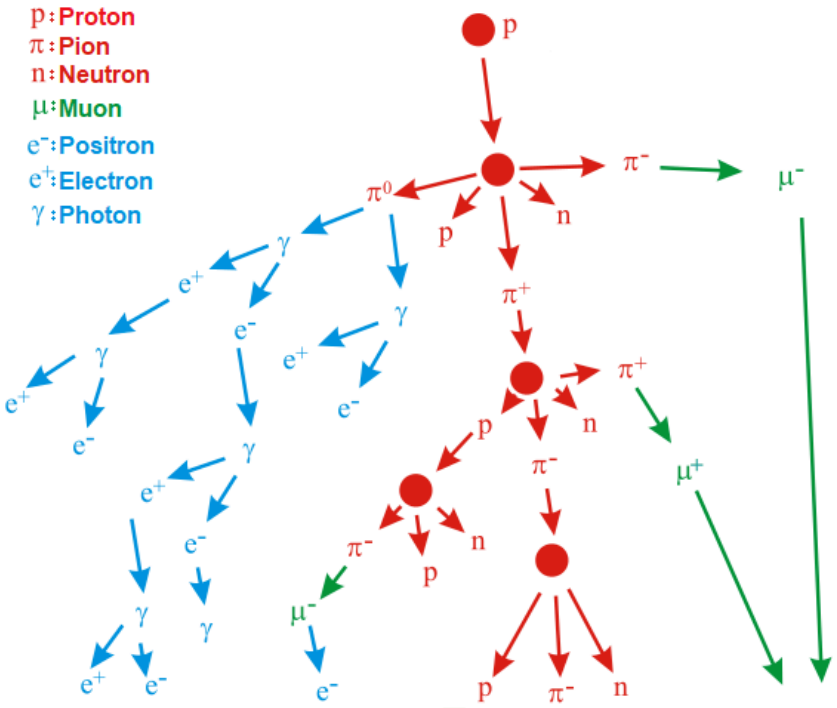

Figure 1.2.2: An example of an air shower with different ways to generate muons and neutrinos.

$$\begin{aligned} \pi^+ &\to \mu^+ + \nu_\mu \to e^+ + \nu_e + \bar{\nu}_\mu + \nu_\mu \\ \pi^- &\to \mu^- + \bar{\nu}_\mu \to e^- + \bar{\nu}_e + \nu_\mu + \bar{\nu}_\mu \end{aligned} \tag{1.2.1}$$

From this decays the flavor ratio from atmospheric neutrinos spectrum can be derived as

$$\nu_e : \nu_\mu : \nu_\tau = 1 : 2 : 0\,, \tag{1.2.2}$$

where the distinction between neutrinos and anti-neutrinos was not made.

GZK-neutrinos: The GZK cutoff named after K. Greisen, G. T. Zatsepin, and V. A. Kuz'min who postulated the interaction of protons with photons of the cosmic microwave background [13, 14] forming Δ^+ resonances, is also an origin for high energetic neutrinos of the order of $10^{16}\,\text{eV}$ to $10^{18}\,\text{eV}$ [15], which are energies of interests for the neutrino astronomy. The chain of reactions from a proton p interacting with a microwave background photon γ runs as follows.

$$\begin{aligned} p + \gamma \to \quad \Delta^+ &\to p + \pi^0 \\ \pi^0 &\to \gamma + \gamma \end{aligned} \tag{1.2.3}$$

$$\begin{aligned} p + \gamma \to \quad \Delta^+ &\to n + \pi^+ \\ \pi^+ &\to \mu^+ + \nu_\mu \\ \mu^+ &\to e^+ + \nu_e + \bar{\nu}_\mu \end{aligned} \tag{1.2.4}$$

Cosmic neutrinos appear with energies from $10^{15}\,\text{eV}$ and there are only hypotheses where and how these neutrinos are generated. Some likely sources were introduced in chapter 1.1. However, the most plausible hypotheses is the hadronic model, where protons are accelerated by a shock acceleration, which means that charged particles are reflected and accelerated in strong magnetic fields. These high energy particles are, for example, protons, which then interact with photons and delta resonance (Δ^+) are spawned and decaying as introduced in in equation 1.2.3. Protons also can interact with a heavier nucleon N.

$$p + N \to \pi + X\,, \tag{1.2.5}$$

where X is the hadronic component and π is either neutral or positive or negative charged and decaying to neutrinos as in equations 1.2.1.

So to detect neutrinos, it is necessary to detect the secondaries from the interaction. For very high energetic leptons there is a helpful phenomenon in physics called Cherenkov effect. The Cherenkov effect appears if charged particles move faster through a medium than the speed of light c_m. This is possible because only in vacuum nothing is as fast as light. In a medium with a refractive index of n the light only moves at a fraction of the speed of light in vacuum c and the velocity of particles v can be faster [16]. If this happens the medium gets polarized by the electric field of the particle and causes

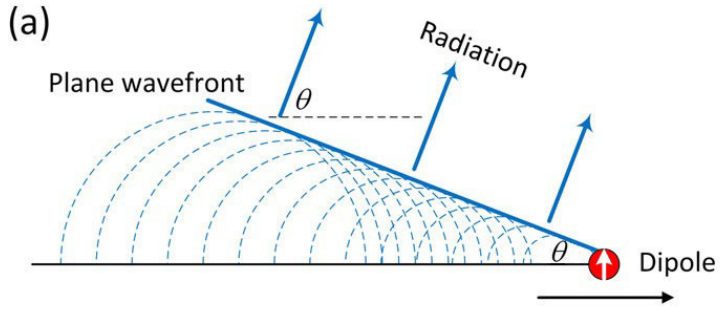

Figure 1.2.3: Radiation of the Cherenkov radiation at a uniform velocity.

radiation due to the de-excitation of the excited electrons. Normally, when the particles are moving slower than the light this radiation interferes destructive and vanishes. With faster particles causing the radiation is interfering constructive and photons get emitted. The charged particle will emit the photons in the form of a cone with an opening angle relative to the direction of the particle. A sketch of this process is shown in figure 1.2.3[2].

The opening angular θ can be calculated with the help of the particle's speed $v_p = \beta \cdot c$, where β is the ratio between v_p and c, and the reflective index n as:

$$\cos(\theta) = \frac{c \cdot t}{\beta \cdot c \cdot t \cdot n} = \frac{1}{\beta \cdot n}. \tag{1.2.6}$$

The minimal needed kinetic energy E_C of a charged particle to produce Cherenkov radiation can be calculated by:

$$E_{kin} = (\gamma - 1)\, m_0 c^2 = m_0 c^2 \left(\frac{1}{\sqrt{1-\beta^2}} \right) > E_C = m_0 c^2 \left(\sqrt{\frac{n^2}{n^2-1}} - 1 \right), \tag{1.2.7}$$

with m_0 as the invariant mass of the particle and the Lorentz factor $\gamma = {}^1/\sqrt{1-\beta^2}$. Which corresponds to a needed energy for an electron in the ice, with a reflective index $n_{ice} = 1.31$, to $E_{C,\,e^-} = \sim 0.28\,\mathrm{MeV}$.

[2]Taken from: https://media.springernature.com/lw685/springer-static/image/art%3A10.1038%2Fs41598-017-08705-4/MediaObjects/41598_2017_8705_Fig1_HTML.jpg

1.2.1 The IceCube Observatory

Neutrinos are helpful messenger particles to have a deep look into the universe but due to their tiny interaction cross-section, a huge detector is necessary. With the IceCube Observatory located at the geographic south pole, the largest neutrino detector was built.

1.2.1.1 Present IceCube Observatory

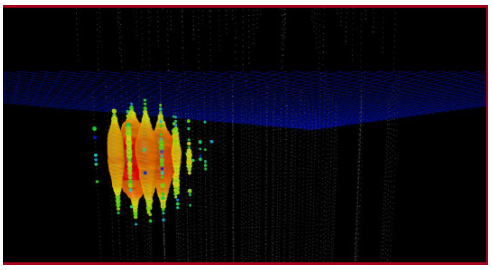

(a) Signature caused by an electron neutrino or neutral charged current.

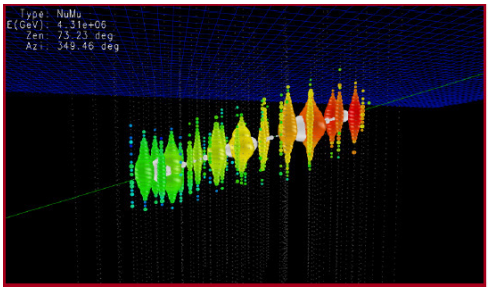

(b) Signature caused by a muon neutrino.

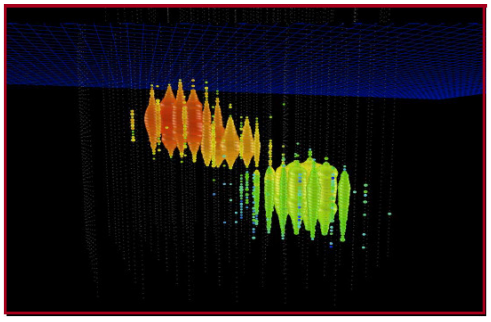

(c) Signature caused by a tau neutrino.

Figure 1.2.4: Different signatures of energy deposition in the IceCube detector volume. The color code stands for time of detection (red: early detection, blue: later detection).

With a volume of roughly $1\,\mathrm{km}^3$, the IceCube observatory is large enough to detect a few high energetic neutrinos per year. The detector is instrumented with 5160 digital optical modules (DOMs), fixed on 86 strings installed in the ice in depths between 2450 m and 1450 m. The DOMS have a gap of 17 m between each other on a string and a spacing of 125 m between the stings [17]. An overview of the IceCube observatory is shown in figure 1.2.5. The detector was completed and is continuously operating since 2010. In the previous chapter 1.2 the interactions between neutrinos and ice particles were described, with the result that the produced leptons generate Cherenkov light. This light is detected by the deployed DOMs. Each DOM contains a ten-inch photomultiplier (PMT, further information about PMTs can be found in chapter 1.2.2) which is facing downwards. Since the Ice has a very low only optical activity the Cherenkov light and PMT background noise (details in chapter 1.2.2.3) will trigger the installed PMTs in the DOMs. The information about the interacting neutrinos passive detected via the Cherenkov light are the direction, energy and arriving time of the neutrino. The energy can be estimated from the sum over the detected light in each DOM, and the direction can be reconstructed with the help of the arriving time of the light in each DOM.

The three different neutrino flavors produce different patterns in the detector volume, shown in figure 1.2.4.

A cascade (1.2.4a) is the structure detected most often in the IceCube volume, this can be explained by the fact, that two different reactions can cause a cascade. The first one is the neutral current process entered by all neutrino flavors, see equation 1.1.2. In this interaction, a neutrino scatters with a nucleus and only transfers some energy. The second kind of interaction that causes a cascade is an electron neutrinos scattering with a nucleus and exchanging a $W^{\pm}$ boson and producing an electron, almost all the energy of the neutrino

is deposited in the volume of the detector and is therefore easy to reconstruct. In another charged current interaction a muon neutrino ν_μ will produce a so-called track (1.2.4b) which can be even longer than the diameter of the detector, so energy reconstruction is more difficult but the angular resolution is better than with electron neutrinos. A so-called double bang (1.2.4c) is the result of a tau neutrino. The neutrino produces a tau lepton, this tau will cross the ice for a few hundred meters and will decay in another particle. Electron and muon signatures are well understood and seen regularly, a double bang was not detected yet. The color coding in figure 1.2.4 is the following:: red bubbles are early, blue bubbles are later in time. One can also see the deposited energy in the detector by the size of the bubbles.

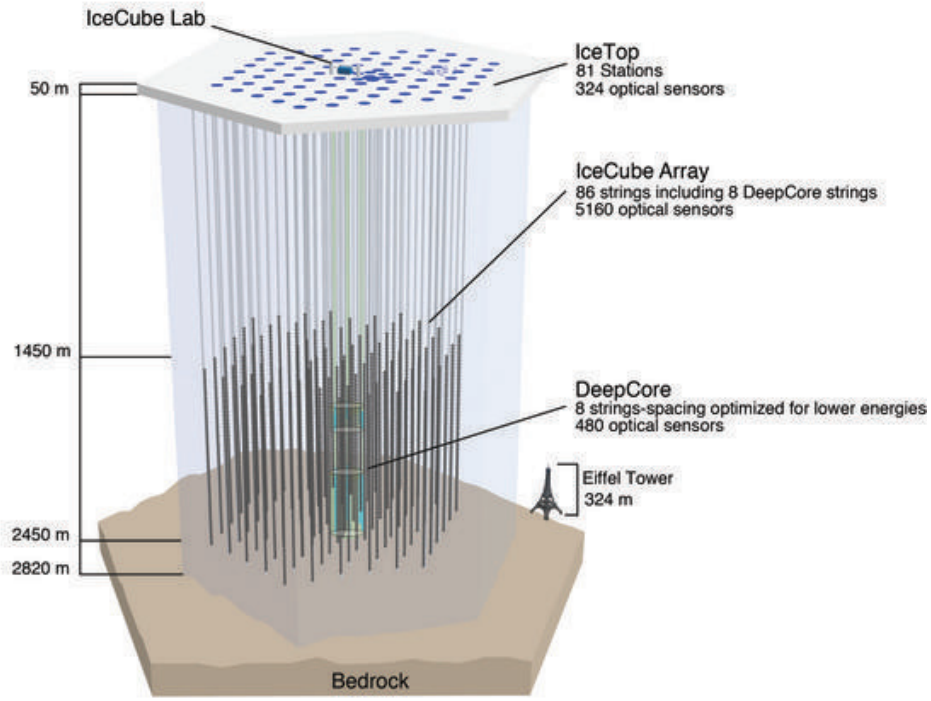

Figure 1.2.5: A sketch of the IceCube detector built in the deep ice of the South Pole with 5160 digital optical modules on 86 strings [17].

1.2.1.2 IceCube Gen2

Since the IceCube detector is working well, it would be nice to get more events per year and also get better results for the reconstruction of energy and angular of the highest neutrinos, therefore an expansion of the current detector is planned. The idea is to increase the volume of IceCube is to deploy roughly the same amount of additional strings into the ice with a larger spacing. The Gen2 detector, in the end, should have a volume of 5 to 10 km^3. A sketch of a possible string arrangement Gen2 is shown in figure 1.2.6, the final string layout was not known by the time of writing. The red part in the figure shows the volume of the current IceCube observatory and the outer blue is the planned IceCube Gen2 volume [18]. This will improve the angular and energy resolution and will provide a higher probability to detect high energetic neutrinos. To improve this even further the deployed module for IceCube Gen2 should also be refined. Therefore four different kinds of improved digital optical module are under development: An updated version of the current IceCube DOM, a module which contains two PMTs facing in opposite directions named D-Egg [19], a thin module which has wavelength shifting properties (WOM) [20] and a module with 24 three-inch photomultiplier facing in all directions the mDOM [8]. The next chapter will provide more information about the mDOM.

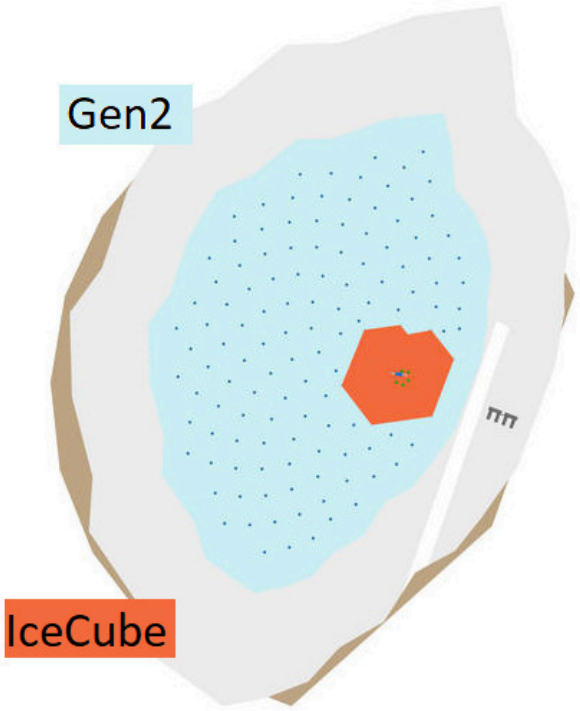

Figure 1.2.6: A rendered image of a possible configuration of the IceCube-Gen2 experiment. In red the present IceCube observatory volume [18].

1.2.1.3 The multi photomultiplier digital optical module

The multi photomultiplier digital optical module is a promising candidate for the IceCube Gen2 (chapter 1.2.1.3) and has been under development for 5 years at the University of Erlangen and in detail described in the Ph.D. thesis [8]. The mDOM features 24 three-inch photomultiplier facing in all directions and thus covers $4\,\pi$. The current layout highlighting its constituents is shown in figure 1.2.7.

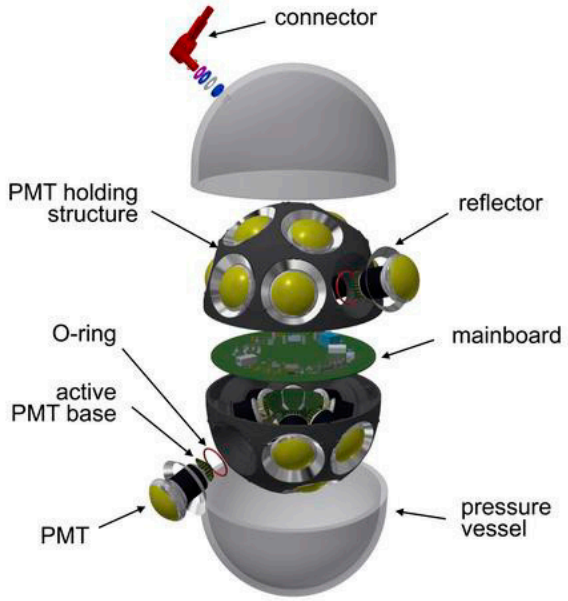

Figure 1.2.7: Exploded view of the mDOM, the PMTs are with the reflector mounted on a black plastic structure inside the glass vessel.

The pressure resistance glass sphere is with its 14 inches in diameter a bit larger than the sphere of the deployed IceCube DOM, so that all PMTs can fit inside. The 24 PMT are placed in a 3d printed holding structure which comes in two parts each one carrying 12 PMTs. Around the photocathodes of each PMT a so-called reflector is mounted, a bend aluminum stripe which increases the frontal photosensitive area of the PMT. The free space between the glass vessel and the holding structure together with photomultiplier is filled with optical gel to reduce the refractive index difference between the PMT and the glass. This also prevents total reflection inside the glass. Due to the high number of photomultipliers, there is not much space inside the module. To fit in all PMTs and the needed hardware and also provide the needed stability, a slightly cylindrical form for the pressure vessel was needed. This design does not require wider drilling hole, which would increase the costs of Gen2 dramatically. The gained space is used for the electrical components. Each PMT is attached to an active base, where the high voltage is generated by a Cockcroft-Walton chain to consume less power. These active bases also digitize the signal of the observed data. The main board in the middle of the module is collecting all the data and sends it to the surface.

Several upgrades are being discussed at the time of writing to improve the, mDOM for example, shorter PMTs could be used to provide more space in the inside for the

electronic components and LEDs should be added on to the holding structure to define the orientation of the DOM in the drilled ice hole.

When comparing the mDOM with the IceCube DOM major advantages are in favor of the mDOM. One of these advantages is the effective area which can be described as the equivalent geometric area of the device assuming 100% efficiency [8]. As shown in figure 1.2.8 photons which arrive at the bottom part of the module the DOM has a slightly higher effective area than the mDOM because the 10 inch PMT is facing in this direction. The mDOM, however, has an almost uniformly high effective area regardless of the arriving-point of the photon.

The other point where the mDOM outperforms the single PMT DOM is in terms of directional information, due to the 24 photomultipliers of the mDOM. Each of these 24 PMTs collects information on his own and can be read out separately so when light hits the mDOM not only one PMT will detect a photon but several will do. Because of that, the mDOM provides a lot more information about the angle and direction of the light than the one PMT in the IceCube DOM. By taking the data from one single mDOM it is theoretically possible to reconstruct the direction of a light beam.

Additionally, the mDOM has a better photon-counting that the DOM, as different PMTs are detecting the arriving photons, their numbers and arriving times can be reconstructed more easily, cause the photons are distributed on more PMTs and not only detected by a single photomultiplier. This also provides a better performance with regard to saturation for the mDOM.

1.2.2 Photomultiplier

Photomultiplier tubes (PMT) are crucial in the IceCube observatory and in this thesis. This chapter will provide the needed information about photomultipliers, working principle and explains the two operating modes as well as the background measurable while using them.

The work in this thesis will concentrate on the 3 ” PMTs which are intended for the use in the mDOM namely the R-12199-02. A picture of this kind of PMT can be seen in figure 1.2.9a.

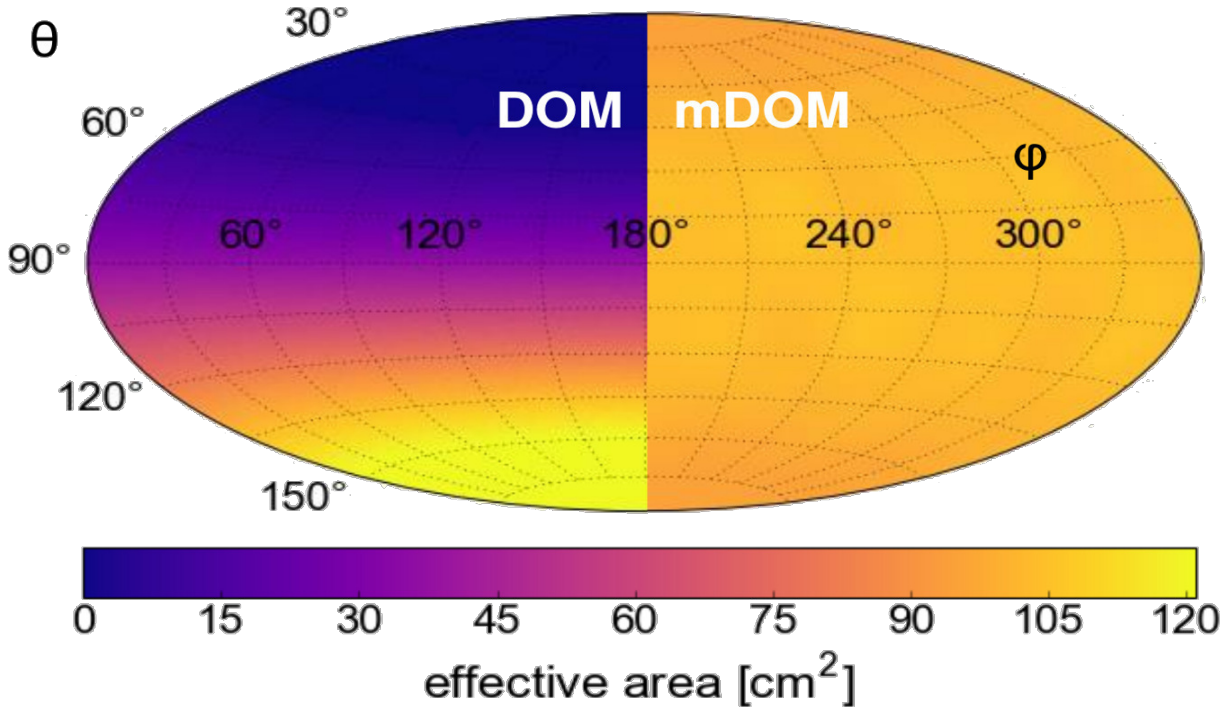

Figure 1.2.8: Comparison of the effective area of the DOM (left) and the mDOM (right) [8].

1.2.2.1 Working principle

A photomultiplier is built from a photocathode, several dynodes, and a collecting anode. In figure 1.2.9b a sketch of a photomultiplier is shown and in figure 1.2.9a an actual picture of a PMT is shown. There are two different methods to power the PMT one either put the photocathode on negative high voltage and the anode on ground or the photocathode is on ground and the anode is on positive high voltage [22]. In both cases, there is a negative gradient from the cathode to the anode. So the photocathode always is on the most negative potential and the anode is on the most positive potential. The potential of the metallic dynodes between them follows the gradient an get more positive to the anode with set voltage differences. In the interior of the PMT is a vacuum, so that the electrons do not interact with any gas molecules.

When photons hit the photocathode, which is made from a semiconductor an electron is released due to the photo effect, and gets reflected inside the semiconductor and finally emitted into the vacuum (see figure 1.2.9). This electron is onto the first dynode due to the voltage gradient accelerated. While hitting the first dynode the electron deposits energy in the material via inelastic scattering and secondary electrons are emitted from the dynode. The secondary electrons are accelerated to the next dynode and more secondary electrons are generated. This process continues until all generated electrons hit the anode. With this principle, single photons are converted to millions of electrons which produce a measurable charge pulse at the end. The multiplication factor, called gain, is explained in more detail is in chapter 1.2.2.4. The duration in time of the voltage pulse at the end of the amplification process determines the signal length (FWHM). The timing of the pulses is also not perfectly stable in time due to the transit-time spread (TTS) of the PMT [24].

(a) A photo of the developed photomultiplier R-12199-02 by Hamamatsu.

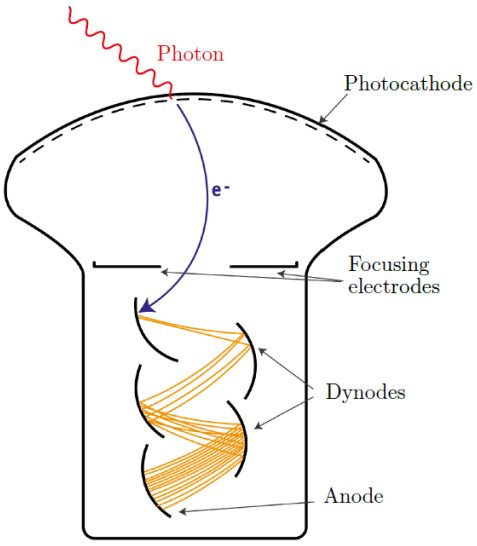

(b) A rendered image of the inside of a PMT [21].

The TTS indicates the different transit times of electrons generated at the cathode. The transit time describes the time a PMT needs to generate a signal after a photon triggered the emission of an electron on the photocathode, so it is deduced by the travel time of the electrons inside the PMT. If the electron is generated in the center of the photocathode is arrives faster at the first dynode than generated at the edge of the photocathode, see figure 1.2.10.

The different voltage setup of the PMT does not affect the general principle of a photomultiplier, it only differs in the way the readout process can be done. A PMT provided with negative high voltage has the advantage that there is no high voltage at the anode and the readout of the pulses is straightforward. The downside of this method is the higher noise level caused by the cathode on high voltage. The different sources of noise inside a PMT are explained in the next chapter (1.2.2.3). If the anode is on high voltage though, the noise is low, but the readout process is more complicated because the generated voltage peak has to be isolated from the high voltage baseline of the anode.

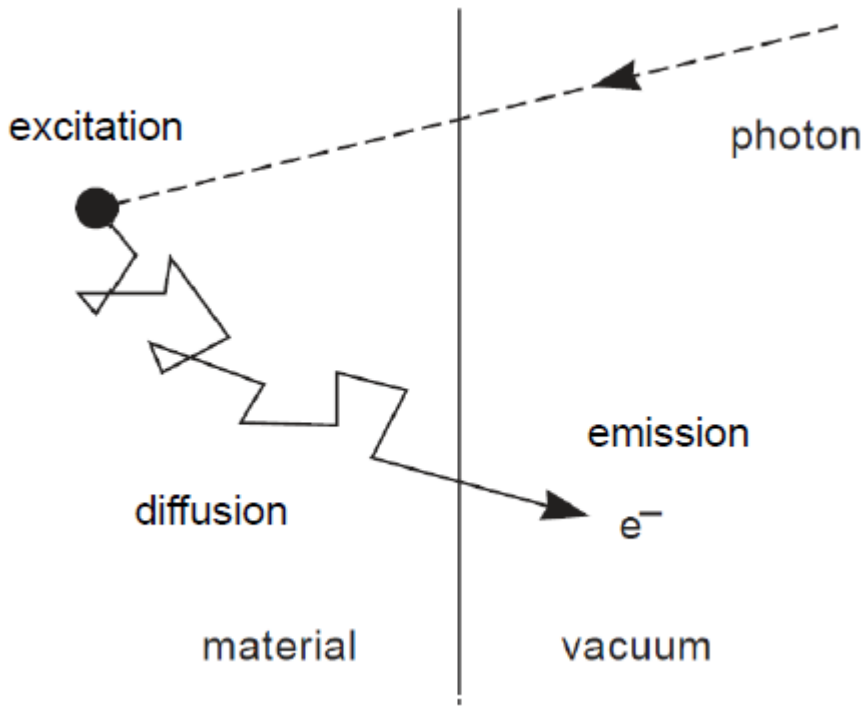

Figure 1.2.9: Visualization of conversion of a photon into an electron in the photocathode, the most important steps are the absorption of the photon, the diffusion of the electron inside the cathode and its emission from the surface. It is not necessary that the electron is emitted at the same side at which the photon enters [23].

1.2.2.2 Operating modes

There are two different ways the charge of the anode can be read out to get the signals, either in current or in pulse mode [25].

The current mode is used, when the rate of photons is very high, as the name suggests the electrons arriving at the anode are measured by their generated current with an amperemeter. The charge of all pulses which arrive in a defined time window is integrated resulting in a current value. With this mode, the exact timing of the pulse cannot be measured.

The pulse mode can be used when is low so the pulses arrive separately. With an attached readout device like an oscilloscope, the voltage pulses of the arriving electrons are measured. This mode counts the arriving photons and is able to measure the amplitude, width, area of the pulses and the exact timing. This mode is also useful to look for single photon peaks. With too high frequencies the pulse length of the PMT will increase and

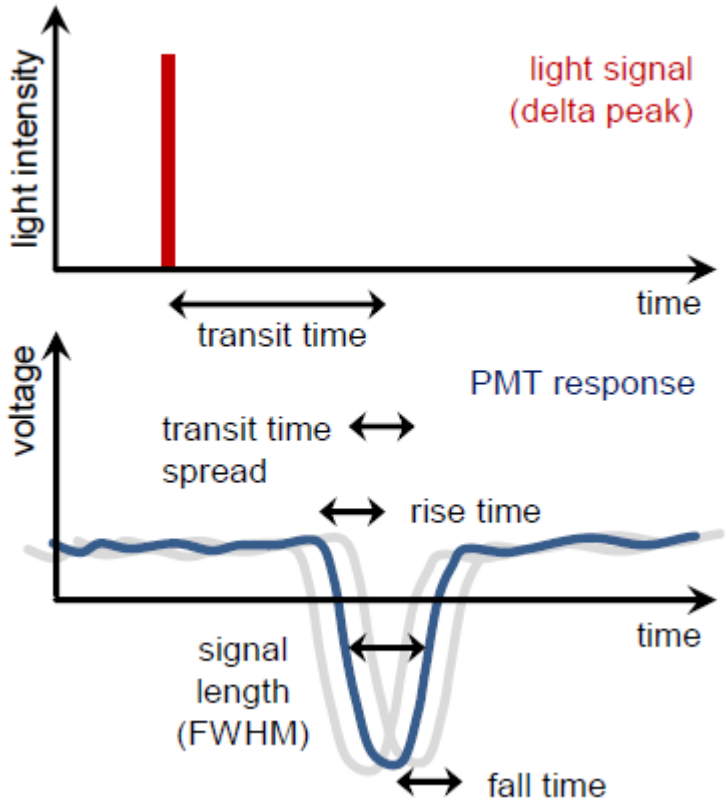

Figure 1.2.10: Explanation of the transit-time spread in a PMT originating from the not spherical surface of the cathode, causing different length from the cathode to the first dynode so different travel times (bottom). Hit time of the photon and the photocathode (top) [8].

pulses cannot be developed separately. A short example is shown in figure 1.2.11. In this work, the pulsed mode is used for all experiments.

1.2.2.3 Dark rate

There are two different kinds of noise which appear in a powered PMT: correlated and uncorrelated noise. That means that even when there is not a single photon hitting the photocathode, the photomultiplier will produce some signals which are called noise or dark rate. The second type of dark rate is the dark current with refers to signal with an amplitude in the range of nanoamps and is a function of the gain [26]. Depending on the used operation mode. In the following, all types of noise are introduced.

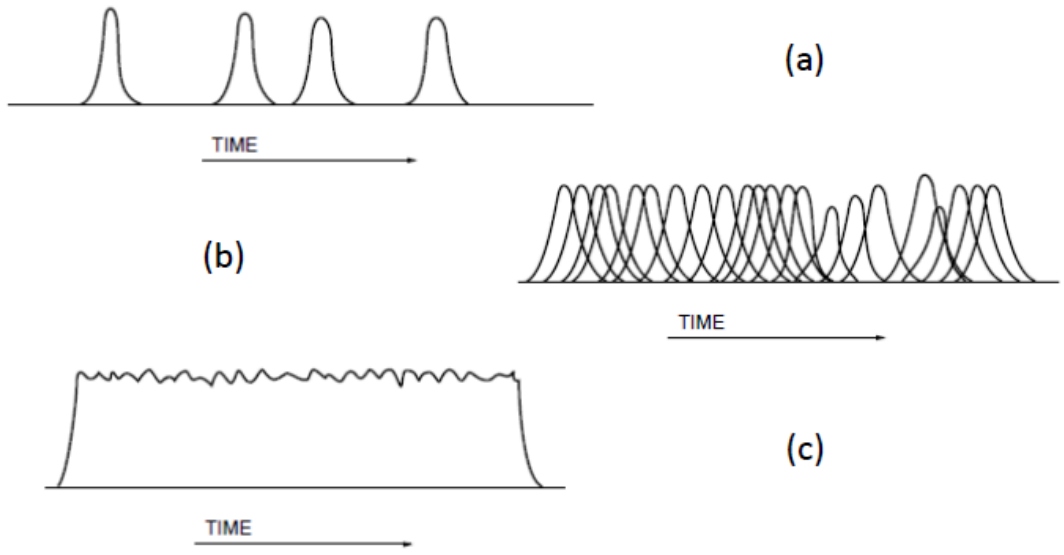

Figure 1.2.11: Examples of signal frequencies measured by a PMT. With a low signal rate where most pulses are measured separately (a) the pulse mode is the recommended operation mode. With a high signal frequency (c) the current mode is advisable. With a frequency like in (b) both modes can be used depending on which property is needed [25].

Uncorrelated background

Thermionic emission

If an electron gets emitted and causes a normal multiplication cascade of electrons, without a photon hitting the photocathode, it is called thermionic emission, which is the main discrete component of the background. It can't be distinguished between a photon hitting the photocathode and thermionic emission. The rate is increasing with the temperature following Richardson's law.

$$J = AT^2 \exp(-\frac{W_{th}}{kT})$$

where the Richardson constant is $A \approx 6 \cdot 10^5\,\mathrm{Am^{-2}K^{-2}}$, the current density is represented by J , W_{th}stands for the work function, T for the absolute temperature and k is the Boltzmann constant. Reduction of this noise can be achieved by cooling the PMT.

Field emission

The field emission describes a form of the tunneling effect, where electrons can be emitted by the dynodes due to a strong electrostatic field. These electrons can either hit the dynode again or the glass of the PMT and produce scintillation light which then has a probability to hit the cathode. The rate of the field emission depends on the applied voltage of the photomultiplier.

Internal background radiation

In the glass of the PMT housing, some radioactive isotopes are localized, such as the isotope ^{40}K. The decays of this isotope contribute also to the dark rate, either by ionizing particles which hit the glass and causes Cherenkov radiation or by photons of radioactive decays hit the photocathode or electrons from beta decays hit the dynodes and produce a signal.

Excitation

If the PMT was exposed to light before using it, particles of the photocathode, the leftover gas inside the PMT and the glass of the PMT are excited. During the de-excitation of the particles, photons can be emitted producing higher dark rate several hours after powering up the photomultiplier. This phenomenon can be reduced by waiting a few hours before using the PMT, otherwise, the dark rate is up to one order of magnitude higher than normal.

Correlated background

In contrast to the uncorrelated background, the correlated background is, as the name suggests, additional pulses related to the real pulses of the PMT or pulses generated by mechanisms described before. These so-called early- or afterpulses appear while the PMT is operated and occur shortly before or after the real pulse [26].

Early pulses

Early pulses also called pre-pulses appear when photons don't interact with the photocathode and hit the first dynode instead, causes there an emission of an electron. This electron will generate a smaller pulse at the anode and arrives earlier than an ordinary pulse would arrive because the photon travels faster from the cathode to the first anode than the electron. A typical time value of an early pulse depends on the length between cathode and dynode, being less than one to a few nanoseconds.

Late pulses

Late pulses are produced by electrons hitting the first dynode without producing secondary electrons but get back-scattered. This electron is then again accelerated onto the first dynode by the electric field and generate secondary electrons which follow the normal trajectory in the PMT and produce a pulse at the end. This pulse looks like a regular pulse but is delayed in the order of nanoseconds.

Afterpulses

Afterpulses appear form nanoseconds to a few microseconds after the regular pulse. The main reason for their appearance is ionization of gas atoms by electrons in the non-ideal vacuum inside the PMT. The emitted electron is accelerated towards the first dynode as usual but the now positive charged atom will be accelerated back onto the cathode and will release several electrons from the photocathode. These electrons result in a pulse, which is detected after the first pulse.

1.2.2.4 Single photoelectron spectrum

When a PMT is used in pulsed mode it is important to know how many photons correspond to a measured peak, therefore, a calibration of the photomultiplier is needed. Operated in pulse mode the deposit charge from the secondary electrons on the anode can be measured by this peak. In figure 1.2.12

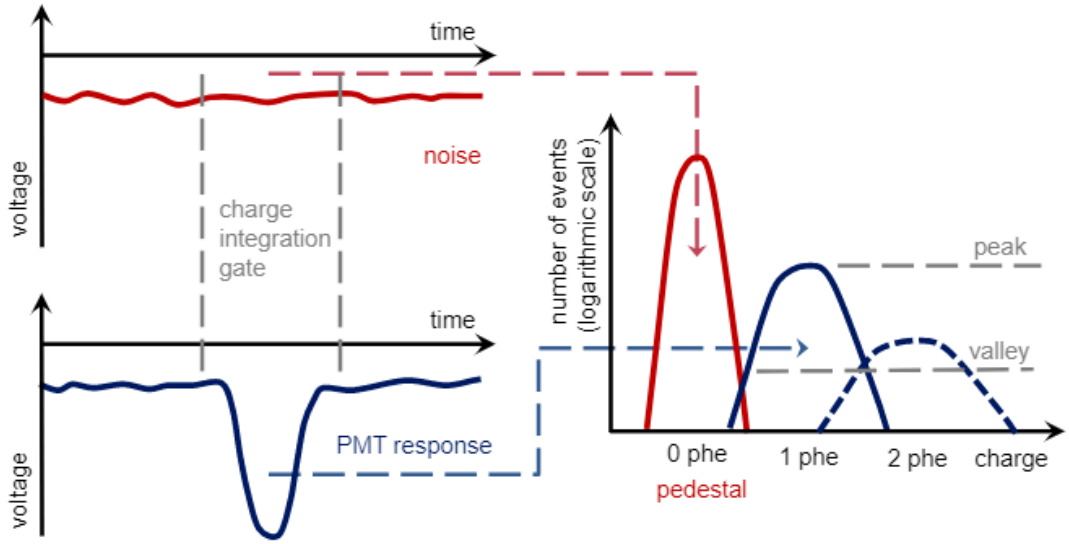

Figure 1.2.12: The pedestal in red (right) shows the integrated baseline of the PMT signal (left) in the defined charge integration gate, the blue lines indicate the integrated PMT signals (left) sorted into different photoelectrons (right) [8].

the principle is illustrated. To ensure that only a photon pulse is integrated and not background or afterpulsing, a fixed integration time window is defined relative to the trigger. The mentioned trigger is provided by an external light source which is focused on the PMT, with a defuser in between. To ensure to obtain a single photoelectron (SPE) spectrum the light source is operated with a low light output level like 0.1 photoelectrons (phe) per pulse. A sketch of a setup can be found in figure 1.2.13.

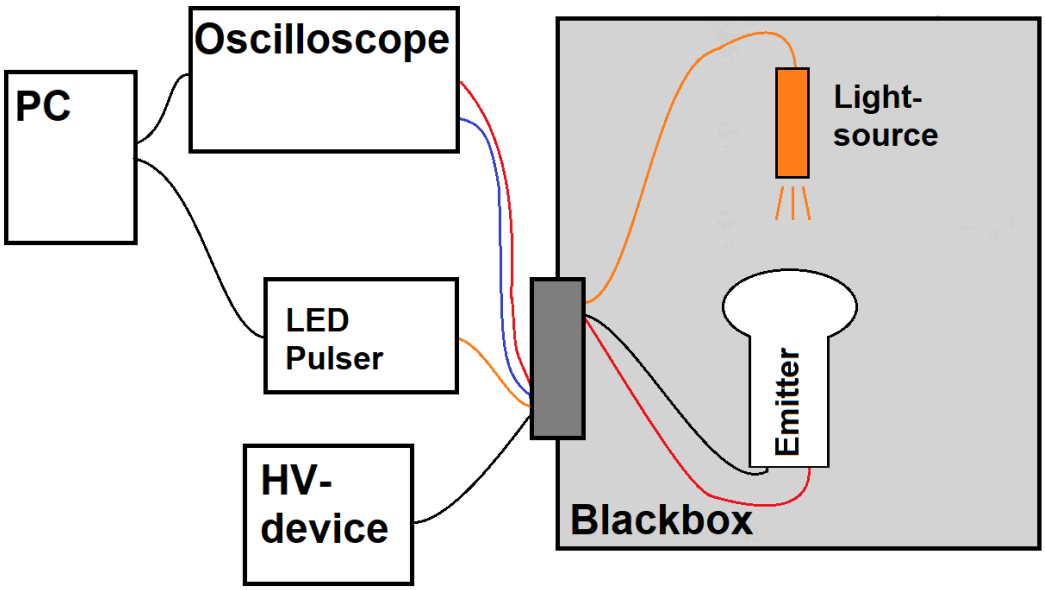

Figure 1.2.13: Sketch of the calibration setup

The taken spectrum can be used to get the PMT properties such as gain and peak to valley ratio. An expected spectrum is shown in fig 1.2.12. The number of measured events are plotted against the number of photoelectrons. The first peak here in red called pedestal corresponds to the baseline without any pulse from the PMT, so zero photoelectrons were detected. The position of this peak defines the origin of the charge axis, the width of the peak corresponds to the noise and gets smaller with a less noisy setup.

The blue peaks represent the photoelectrons the first one is one photoelectron the second one shows the number of 2 phe arrived in the same charge peak, so two electrons were emitted by the photocathode at the same time and so on.

The gain, in pulse mode, G_{pulse} of the PMT can be derived from the presented distribution as

$$\frac{Q_{1\,phe} - Q_{0\,phe}}{e} = \frac{Q_1}{e} = G_{pulse} \tag{1.2.8}$$

where $Q_{0\,phe}$ and $Q_{1\,phe}$ are the positions of the pedestal (0 phe) and the 1 phe peak in the spectrum and e is the quantum charge. To fit this spectrum a model suggested in [27] is described in the following paragraph.

With a pulsed light source like a pulsed LED, we can consider that the number of photons hitting the photocathode is Poisson distributed and also the emitted electrons can be described as a convolution of Poisson and binary processes. That gives us:

$$P\left(N, \mu\right) = \frac{\mu^N \cdot e^{-\mu}}{N!} \quad \text{with} \quad \mu = N_\gamma \cdot QE \cdot C_0 \tag{1.2.9}$$

where N is the number of detected electrons, μ is the mean number of photoelectrons fed into the dynode structure, QE is the quantum efficiency and C_0 is the collection

efficiency of the first dynode. N_γ stands for the mean number of arriving photons at the photocathode.

The multiplication process of a PMT inside the dynode structure can be described as a Gaussian distribution $G_1(q)$, if the secondary emission of the first dynode is large (> 4) and the coefficient of secondary electrons by the first few dynodes is close to one.

$$G_1(q) = \frac{1}{\sigma_1\sqrt{2\pi}} exp\left(-\frac{(q-Q_1)^2}{2\sigma_1^2}\right), \tag{1.2.10}$$

where q is the variable charge, Q_1 the mean SPE output charge and σ_1 the corresponding standard deviation. If the first dynode collects more than one photoelectron the formula 1.2.10 has to be corrected with the assumption that the amplification processes of charges initiated by different photoelectrons are mutually independent as the following:

$$G_N(q) = \frac{1}{\sigma_1\sqrt{2\pi N}} \exp\left(-\frac{(q-NQ_1)^2}{2N\sigma_1^2}\right), \tag{1.2.11}$$

where N is the number of electrons hitting the first dynode. The equation 1.2.11 will give the correct value for $N \to 0$, namely a delta peak as pedestal at zero charge. With the formulas 1.2.9 and 1.2.11 a charge response $S_{idl}(q)$ to N_γ incoming photons can be built for an idealized PMT, eg. without any noise, by conducting the two formulas.

$$S_{idl}(q) = P(N,\mu) \otimes G_N(q) \tag{1.2.12}$$

$$= \sum_{N=0}^{\infty} \frac{\mu^N e^{-N}}{N!} \frac{1}{\sigma_1\sqrt{2\pi N}} \exp\left(-\frac{(q-NQ_1)^2}{2N\sigma_1^2}\right) \tag{1.2.13}$$

The background processes, described in chapter 1.2.2.3, can be described, with w as probability that a discrete background signal can occur, as

$$B(q) = \frac{(1-w)}{\sigma_0\sqrt{2\pi}} \exp\left(-\frac{q^2}{2\sigma_0^2}\right) + w\theta(q)\alpha \exp\left(-\alpha x\right), \tag{1.2.14}$$

$$\approx \frac{1}{\sigma_0\sqrt{2\pi}} \exp\left(-\frac{(q-Q_0-Q_{shift})^2}{2\sigma_0^2}\right) \tag{1.2.15}$$

where σ_0 describes the width of the pedestal induced by low-amplitude continuous background, α is the exponential decrease of the discrete background probability with increasing amplitudes, and θ is a step function $\theta(q) = \begin{cases} 0 & q < 0 \\ 1 & x \geq 0 \end{cases}$. Equation 1.2.15 is an approximation for low noise and $1/\alpha \ll Q_1$ where discrete processes contribute in the form of an effective pedestal shift $Q_{shift} = w/\alpha$ from its initial position Q_0.

A realistic response charge distribution $S_{real}(q)$ can be considered, when a convolution of the background (equation 1.2.15) with the response function of an idealized PMT (equation 1.2.13) is done, with the assumption of low noise and high values of μ, it can be simplified to:

$$S_{real}(q) \approx \left\{ \frac{1-w}{\sigma_0\sqrt{2\pi}} \exp\left(-\frac{(q-Q_0)^2}{2\sigma_0^2}\right) + w\theta\left(q-Q_0\right)\cdot\alpha\exp\left(-\alpha\left(q-Q_0\right)\right) \right\} e^{-\mu} + \sum_{N=1}^{\infty} \frac{\mu^N e^{-\mu}}{N!} \cdot \frac{1}{\sigma_1\sqrt{2\pi N}} \cdot \left(-\frac{(q-Q_0-Q_{shift}-NQ_1)^2}{2N\sigma_1^2}\right). \quad (1.2.16)$$

The final equation (1.2.16) can now be used to fit and characterize the charge spectra. For high pulse intensities the noise and pedestal become negligible, so a single Gaussian curve can be used to fit the resulting spectrum.

Chapter 2

Preparation

The mDOM features 24 PMTs in a small volume and to understand the behavior of these photomultipliers is of great importance, as well as that the background should be as low as possible. With the additional knowledge about PMTs, the stable work the mDOM can be guaranteed. The following part of this thesis presents the experiments which were done to investigate the behavior of photomultipliers operating near each other. Particularly the increasement of the rate of a PMT will be studied, the origin of the electron or photon radiation will be sought after and the properties of these emitted particles will be examined.

2.1 Measurement devices and components

Before diving into the measurements of this work, it is necessary to introduce the most important devices and objects which were used during the measurements for this work.

- **The blackbox:** As explained in chapter 1.2.2 a photomultiplier is very light sensitive and can only be used in an extremely dark environment. To guarantee this, all measurements took place in a so-called blackbox. Mainly one blackbox was used to run the following experiments, shown in figure 2.1.1a , it was built from a 70 cm × 50 cm × 55 cm metal box. To ensure that the box is light tight, it was covered on the inside with black neoprene. The black neoprene should also absorb any light which is either produced inside the box or sneaked its way into the box. To introduce cables like a glass fiber or high-voltage cables into the box, a photon maze was designed by the working group and the precision mechanics workshop of the institute. It is shown in figure 2.1.1b. The maze was built of black painted

(a) A photo of the used blackbox.

(b) A photo of the photon maze, the wall structure repeats on the backside.

aluminum and features an alternating wall structure inside a metal box. This structure allows cables to bent around the structure to enter the box, but it absorbs light which can only move straight and is almost not reflected from the walls due to their mat black painting. As an additional light protection, the box is always covered by a black blanket.

- **High voltage supply:** To power the photomultipliers, a stable voltage source with a very low noise level and fluctuations is required. The device which was used during the main measurements was the ISEG NHQ 224M high precision dual channel HV module in NIM standard featuring two channels with a positive or negative voltage output of 0 V to 6000 V. A big advantage of this device is the remote control feature which allows to send commands and read data from a computer with a python program.

- **Oscilloscopes:** During the experiments for this thesis two different types of oscilloscopes were used. The first was an oscilloscope with a built-in monitor from Teledyne, namely the Lecroy WaveSurfer 510 with a maximum frequency of 1 GHz and 10 $\frac{\mathrm{GS}}{\mathrm{s}}$, four channels and a variety of intern measurement functions. This oscilloscope stopped working from time to time so another oscilloscope was used.
  Most measurements were done with the PicoScope 6404C with four channels, a resolution of 8 bits at 5 $\frac{\mathrm{GS}}{\mathrm{s}}$ and a bandwidth of 500 MHz. This oscilloscope cannot work as a stand-alone device and has to be connected to a computer, however, the needed measurements has to be written with python code and thereby it is not self-computing.

- **Light source:** A light source was needed for some of the following measurements. To ensure good results this source has to be stable regarding of light intensity, wavelength, and pulse length as well as frequency. One of the used light-sources is the PLS 450 from PicoQuant with a spectrum with a maximum at of 458 nm and a repetition frequency of 2.5 MHz to 40 MHz. This light source has only five different frequency setups so a frequency generator was connected to the PicoQuant to trigger the light pulses.
  Also, a with Python controllable LED pulser produced by mrongen[1] was used. It features an 850 nm LED with an intern trigger which allows pulse frequencies from < 1 Hz up to 25000 Hz and a pulse length down to 120 ps.

- **The photomultiplier:** The studied photomultiplier is a Hamamatsu R12199-02. It has a 3" photocathode with a quantum efficiency with a maximum at$\sim 25\,\%$.

[1] https://mrongen.de

2.2 Calibration of the photomultipliers

As is was introduced in chapter 1.2.2.4, the gain of a PMT has to be calibrated. This is necessary because PMTs are not perfectly equal, so even if two identical photomultipliers are used in pulse mode and the supplied voltage is the same, the multiplication factor of the secondary electrons can be different. For that reason, it is necessary to define a comparable value for each PMT for a defined supplied voltage and trigger level, this is the photoelectron. This value was defined as the number of measured photoelectrons (phe) and has a linear connection to the threshold.

The setup to measure the charge histogram to calibrate the PMT is illustrated in figure 2.2.1.

The light produced by the LED pulser from mrongen is fed into the dark box via a light fiber. To illuminate the photocathode of the PMT homogeneously a defuser is placed between the fiber output and the photomultiplier. To get a good measurement the intensity of the LED has to be low enough to see the pedestal but high enough to get also a good number one and more photoelectrons, in this measurement the LED pulser was set on approximately 0.3 phe. The signal which triggers a LED pulse is also sent to the oscilloscope to start the measurement of a PMT pulse. The PMT is the whole time set on a fixed voltage level of 1000 V. The signal of the PMT is analyzed by the picoscope oscilloscope and the computer. The amplitude, the charge, and leading edge time of the main pulse is measured and saved. With this data, the calibration of a photomultiplier can be done.

First the charge and the phe has to be set in context. Therefore the measured charge

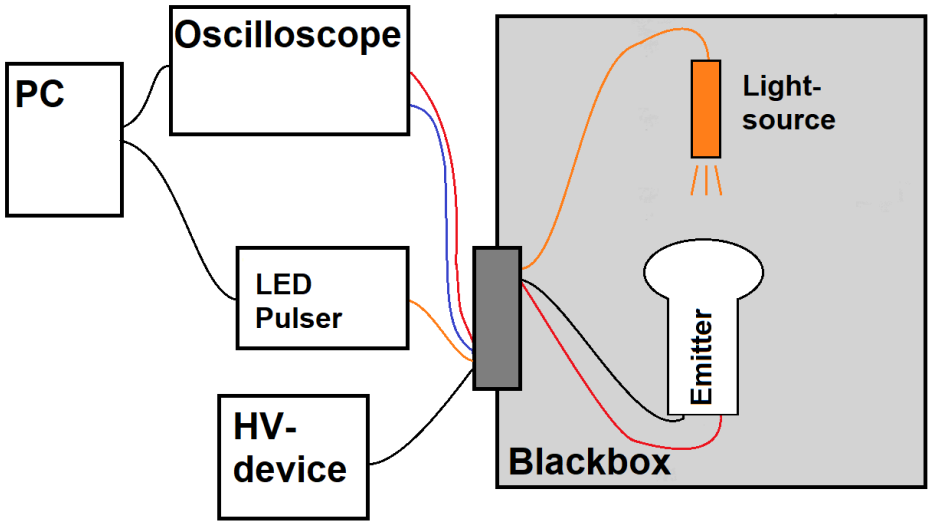

Figure 2.2.1: The used Setup for the calibration with one PMT, the LED pulser from mrongen, and the picoscope oscilloscope.

is plotted on a histogram, figure 2.2.2 and fitted with the equation 1.2.16[2]. The discrete background distribution Q_{sh} is set to zero, otherwise, it would break the linearity between charge and the number of photoelectrons in the interval $0 - 1\,\mathrm{phe}$. With this result and with a calculated mean charge of one photoelectron pulse $Q_{1\,phe} = (1.87 \pm 0.04) \cdot 10^{-13}\,\mathrm{C}$ and the pedestal $Q_{0\,phe} = (7.58 \pm 0.52) \cdot 10^{-15}\,\mathrm{C}$ the gain can be calculated by the equation 1.2.8.

$$G_{pulse} = \frac{Q_{1\,phe} - Q_{0\,phe}}{e} = \frac{(1.79 \pm 0.04) \cdot 10^{-13}\,\mathrm{C}}{1.60 \cdot 10^{-19}\,\mathrm{C}} = 1118750 \pm 25000$$

In this thesis all measurements were done at room temperature 20°C, so the dependence of the gain from the temperature will not be measured.

PMT pulses are measured and separated from the noise by applying a trigger level in the oscilloscope, so every time the PMT[3] signal exceeds the given threshold the oscilloscope measures the pulse. The problem now is that the information about the number of detected photons is given in charge and that the amplitude of the pulse. To transfer

[2]The program to fit the charge histogram was written by M. Unland.
[3]operated in pulse mode

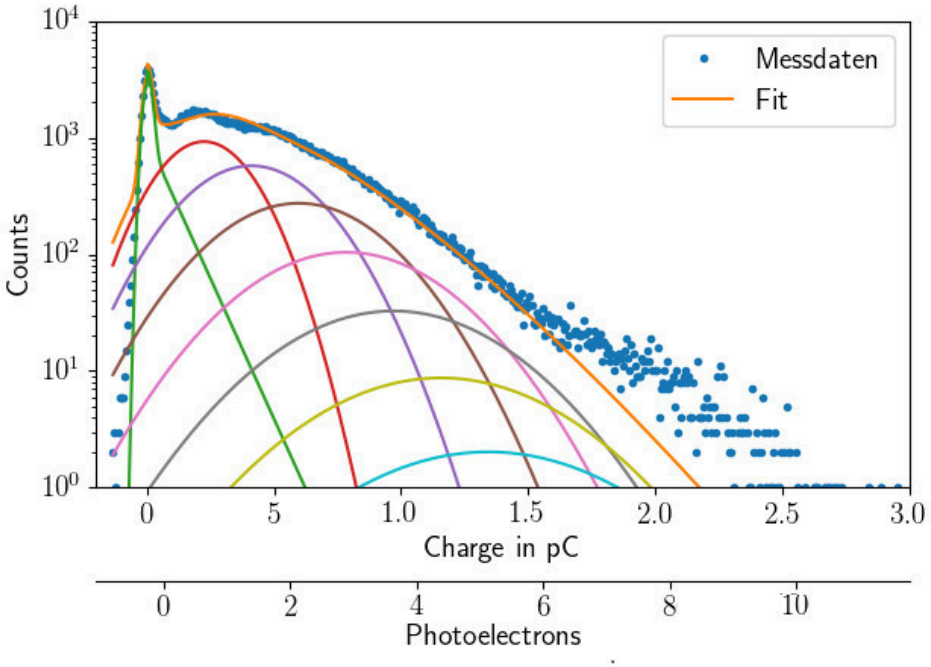

Figure 2.2.2: The charge histogram of the PMT later called Observer. The orange line represents the fit with the equation 1.2.16, the colored Gaussians result from the fit and are representing the deconvoluted phe distributions and the green peak the pedestal including an exponential for the noise.

the trigger level in mV to the corresponding number of photoelectrons, the charge and the amplitude of a pulse are saved simultaneously, and the corresponding charge trigger can be calculated for each amplitude, by applying a cut off mechanism with which the transmission of the charge to the amplitude can be done. [21]. Now calculating the trigger equivalent for voltage threshold in phe the data shown in figure 2.2.3 is obtained. Due to the not perfectly fitted charge histogram, the uncertainties of measurement data is large. Nevertheless, the linear correlation between the trigger level in photoelectrons T_{phe} and Volt T_{mV} is well visible. With the linear fit of $T_{phe} = -0.57\,\frac{\text{phe}}{\text{mV}} \cdot T_{mV} - 0.89\,\text{phe}$ all trigger levels which are set in voltage on the oscilloscopes can be translated into comparable units of photoelectrons. In the following measurements, the trigger level will from now on always be written in units of photolelectrons.

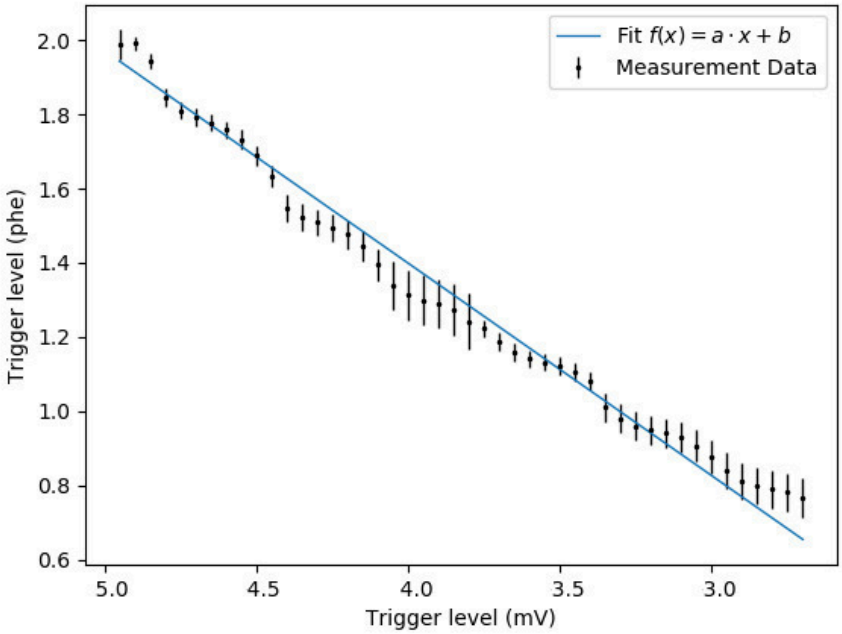

Figure 2.2.3: The trigger level in photoelectrons (phe) plotted against the trigger level in millivolts.

Chapter 3

The emission riddle

3.1 Observation of the emission of a PMT

In the mDOM 24 three-inch photomultipliers are near together in one 24 inch glass vessel. Other experiments with many PMTs packed together in small volume observed an enhanced dark rate of the PMTs when all PMTs were powered on, like the measurement of the collaboration of KM3Net [28] where also a kind of a multi PMT module was developed. The reason and the origin of this phenomenon was not yet clarified. One explanation is the glowing dynode structure [29] another discharges somewhere on the PMT [30]. The cause of this effect should be understood where this increasement comes from and what the photomultiplier do produce that effects other multipliers.

3.1.1 Study of emission of a Hamamatsu R12199-02 PMT

The first experiment was set up to prove that the rate of a photomultiplier is, in fact, higher with another PMTs nearby. Two photomultipliers were used for that: The from now on called Emitter was set on 1000 V negative high voltage, the other one called Observer was working with a positive base also powered with 1000 V. These two different ways to power the PMTs were carefully chosen. The Emitter should represent a PMT from the mDOM, where all PMTs will lay on negative voltage. PMTs on negative voltage have the advantage that the signal on the anode is on ground and therefore it is easy to read out. The Observer, on the other hand, is powered with positive high voltage because this configuration provides less noise and the produced background is more stable. For all following measurements, the Observer will be used with a positive and the Emitter with a negative base.

In this experiment, the rate measured by the Observer were measured with the oscilloscope from Picoscope. To get the rate r of the PMT, which describes the frequency of pulses seen by the PMT in units of $\frac{1}{\mathrm{s}}$. The trigger of the oscilloscope for this experiment and the following will be always measured with a trigger level of 2 mV (0.25 phe). The time between two pulses Δt was measured, but to get fewer fluctuations each point in the following plots is the reciprocal value of the mean of 1000 measured times $\overline{\Delta t}$ between pulses.

$$\begin{aligned} \overline{t_\Delta} &= \tfrac{1}{n}\sum_{i=1}^{n} t_{\Delta i} \qquad \text{, with } n = 1000 \\ r &= \overline{t_\Delta}^{-1} \end{aligned} \tag{3.1.1}$$

The error of the rate Δr is then calculated using the standard error:

$$\Delta r = \frac{1}{n-1}\sqrt{\sum_{i=1}^{n}\left(t_{\Delta i}^{-1} - r\right)^2}\,. \tag{3.1.2}$$

The setup for the first measurement is shown in figure 3.1.1. The procedure was

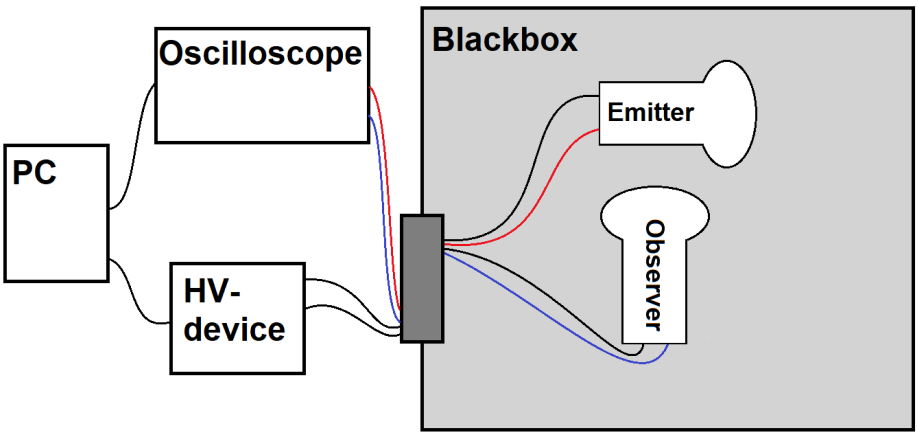

Figure 3.1.1: The standard setup for the rate measurement. The Observer and Emitter are placed in the darkbox and connected to HV and the Oscilloscope. The Observer faces on the dynode structure of the Emitter.

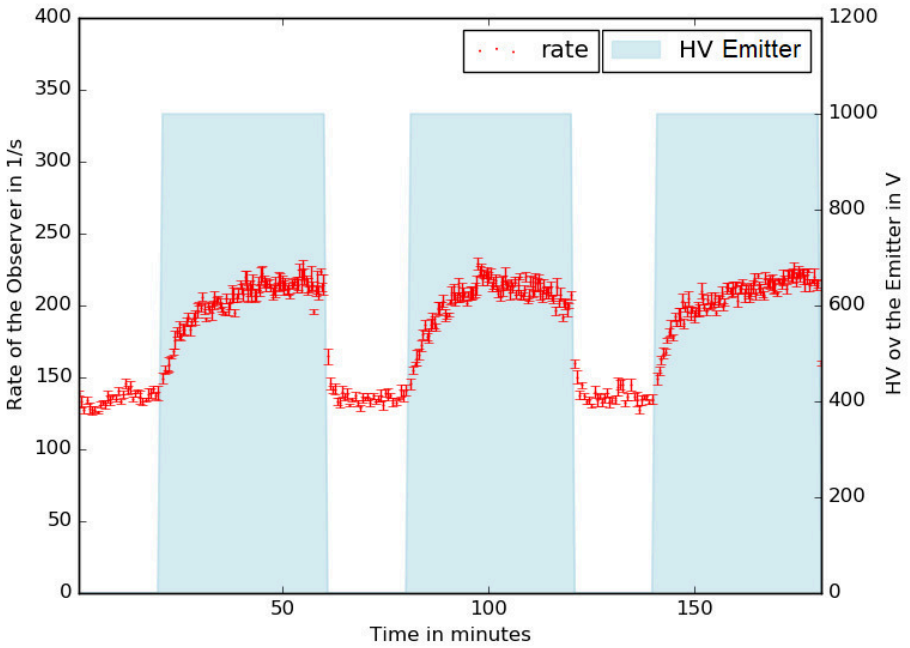

Figure 3.1.2: Measurement of the increasement of the rate. The rate seen by the Observer plotted against the time in minutes.

programmed with Python: The Observer was powered the whole time and the Emitter was turned on and off for 20 minutes each. The measurement data was taken from the Observe facing on the tube part of the Emitter. In the following experiments, the rate of the Observer is measured and shown as red points. The underlying light blue area indicates the times when the Emitter is powered on. In the data (fig 3.1.2) it is clearly visible that every time the Emitter is working the rate seen by the Observer raises about $70\,\frac{1}{s}$ which is about 50 % higher than the normal dark rate of the Observer. Compared with the results from the paper from KM3Net[31] a similar result is achieved. A possible reason for this enhanced rate seen by the Observer is that either on the dynodes of the Emitter or on the glass photons or electrons are generated. Electrons are produced by the photocathode and on every dynode inside the PMT, but due to the strong and well defined electric field gradient in the dynode structure, there is only a small probability that these electrons can escape from the dynnode system. Photons, however, are not influenced by the electric field and could escape easily from the dynode structure. The photons could be generated by electrons hitting and exciting the atoms of the coating of the dynodes. The excited atoms then would relax again and photons are generated during the relaxation. Another possible reason for the enhanced rate could be that the particles are not spawned somewhere on the PMT but e.g. at the base. In figure 3.1.3 the same measurement was performed but the base was covered with black neoprene. The plot of the taken data in figure 3.1.3 shows a similar behavior than before. The increasement of

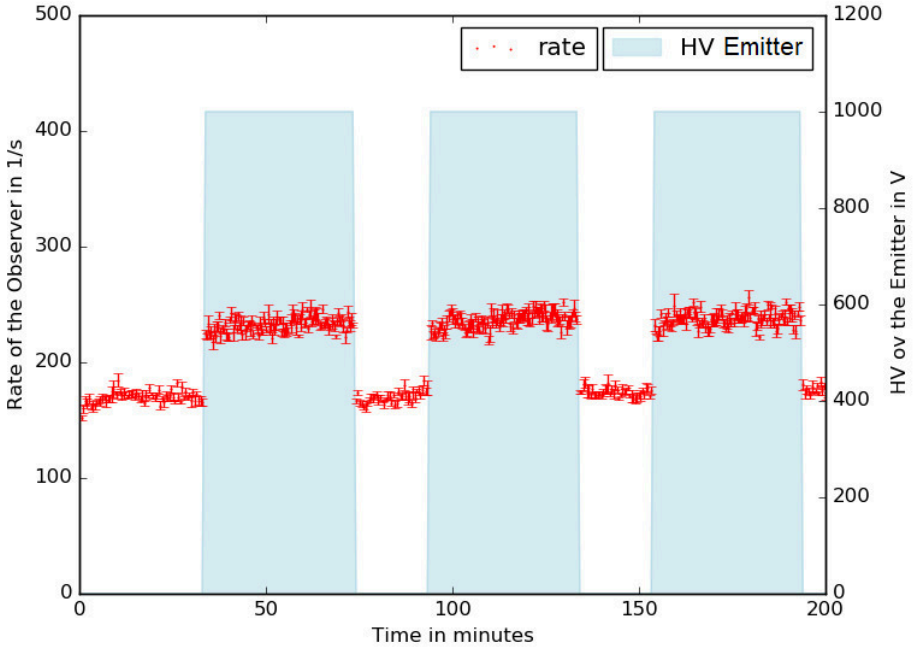

Figure 3.1.3: The measurement of the increasement of the rate with a covered base.

the rate is about 30 %, this difference is caused by the slightly higher dark rate of the Observer. However, this experiment points out that the base is not the main source of the emitted photons or electrons.

In the mDOM, negative bases will be used and for that reason PMTs used with negative HV are observed in this thesis but to make sure that the negative base is not the problem the next measurement features a positive based PMT as the Emitter, to see if only negative but also positive based PMTs are emitting photons or electrons. The result is plotted in figure 3.1.4 and in comparison former measurement the positive PMT causes a higher rate measured by the Observer. An explanation for this higher rate is that here the measured PMT was a different one than in the former measurements because a slightly different pin layout was needed for a positive base; the Observer was the same. Photomultipliers are individually produced so the behavior of each one can be different, and thus the here investigated PMT was glowing stronger. For the investigations in this thesis, the polarity of the Emitter PMT will from now on be negative. This measurement shows that the reason for the emitted photons or electrons are not the different polarities of the PMT base. The PMT "glows" anyway when powered on.

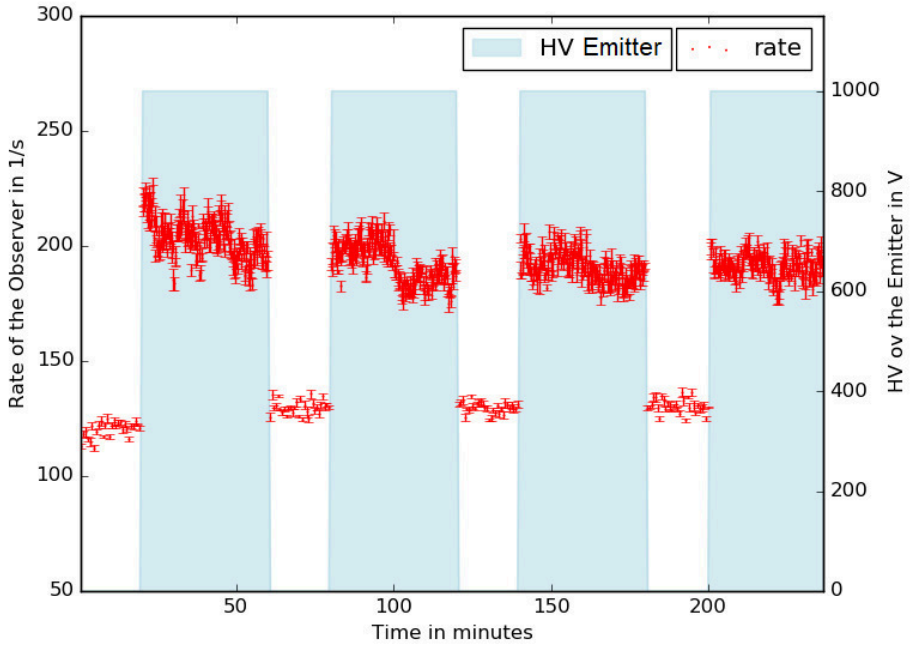

Figure 3.1.4: The measurement of the increasement of the rate with a positive base.

During the measurements, it seemed that the Emitter was "glowing" stronger every time the supplied voltage on the PMT was higher. To prove this hypothesis, the voltage of the Emitter was shifted step by step to another level starting at a supplied voltage of 1400 V decreasing by 100 V after one hour until it reached 800 V. In addition to that,

the rate of the Observer was also measured at 0 V on the Emitter. The mean rate of the Observer at the different supply voltage is presented in figure 3.1.5.

An exponential increase in the mean rate is clearly visible and therefore fitted with the equation $A \cdot \exp(B \cdot x) + C$, which can be seen as a line in the figure 3.1.5. The full equation with all variables is $(6.507 \pm 0.13) \cdot \exp((2.56 \pm 0.02) \cdot 10^{-3} \cdot x) + (135.43 \pm 0.42)$. This relation shows that the supplied voltage has a strong influence on the number of emitted photons, and also leads to the conclusion that the dynode structure or charged glass tube is the origin of the emitted photons.

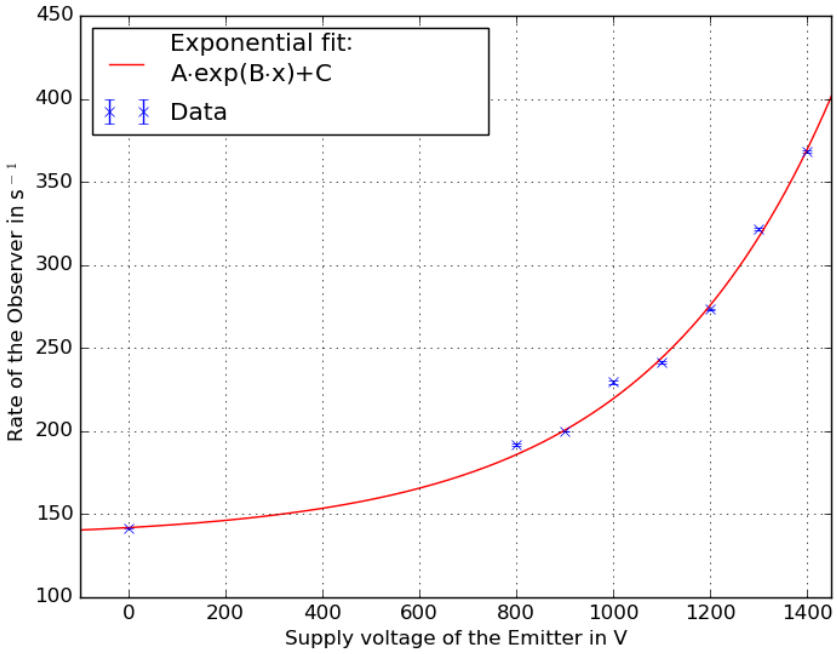

Figure 3.1.5: The rate of the Observer plotted against the supply voltage of the Emitter. An exponential function was fitted to the data and is depicted with a red line.

3.2 Investigation of the emission properties of a PMT

In the previous chapter the "glowing" of the Emitter was proven, but until now it is not clear what kind of particles are emitted and where they come from. In this chapter measurement to figure out if electrons or photons are emitted are performed.

3.2.1 Standard coated Hamamatsu R12199-02

The first measurement in this row was performed with a PMT coated with a black nonconducting material from Hamamatsu. This coating is not transparent for photons nor electrons so everything that could be spawned inside the PMT would be blocked and not visible to the Observer. Only particles generated outside of the tube of the photomultiplier like the base or the pins can cause an increasement of the rate seen by the Observer. The setup used for this is the same which was shown in figure 3.1.1 but this time the Emitter is the described and shown in figure 3.2.1a black coated PMT. The material from which this plating is actually made is not known.

If nothing unforeseen influences the rate of the Observer no increasement whatsoever is expected from the measured rate. When looking at the taken data (figure 3.2.1b) the

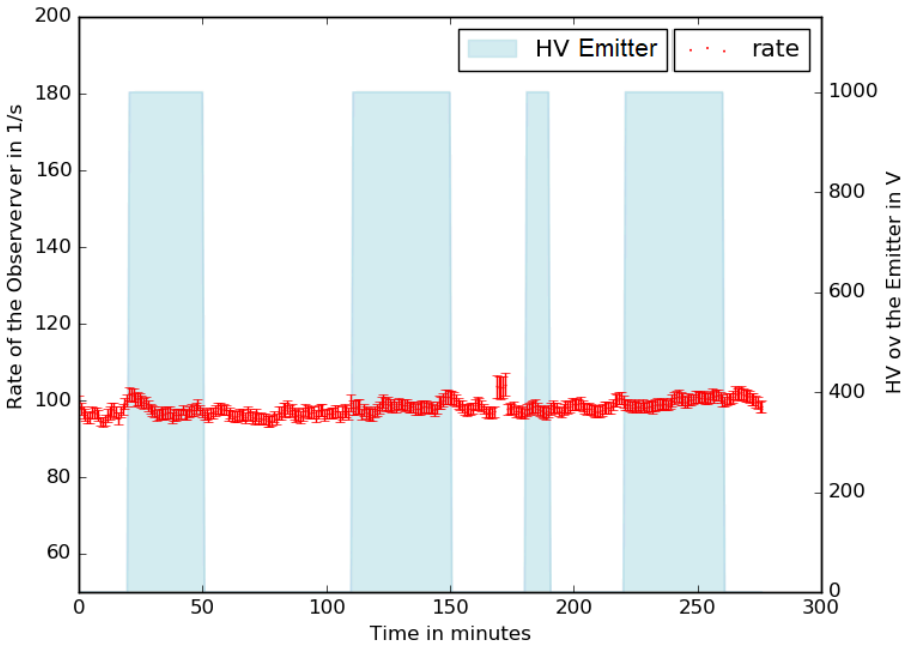

(a) A picture of the PMT coated with the black non-conductingmaterial from Hamamatsu.

(b) The measurement of the rate of the Observer, looking at the Hamamatsu coated PMT.

results agree with the expectations. The rate seen by the Observer stays stable, and the alternating supplied voltage of the Emitter does not influence the rate of the Observer at all. This shows that all particles, either photons or electrons, are produced inside the dynode structure or somewhere on the glass tube of the PMT.

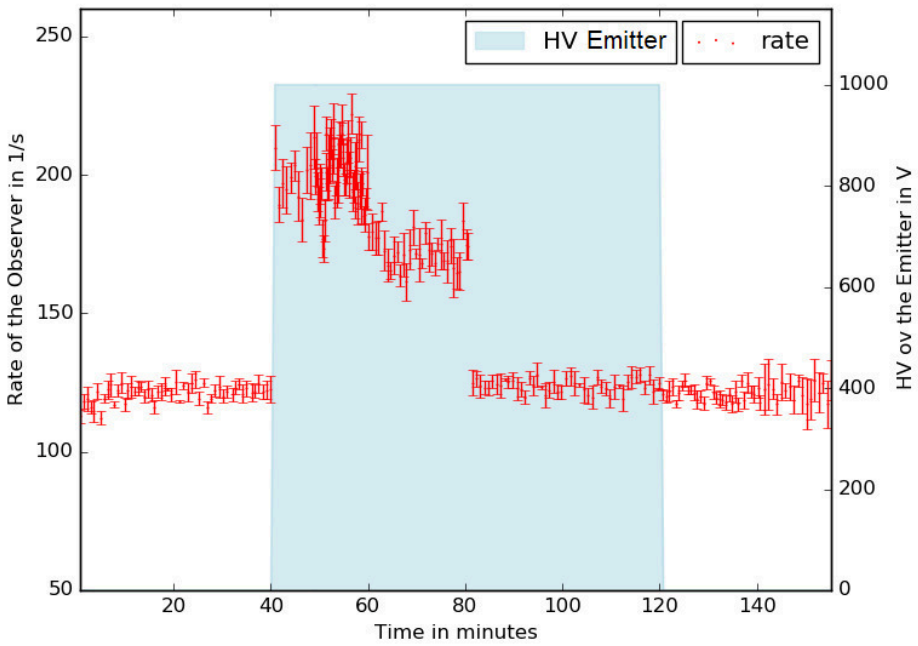

Figure 3.2.1: The plotted data of the measurement of the rate of the Observer. The paper was moved between the two PMTs after 80 minutes.

3.2.2 Study of the emitted particles

Photons are not supposed to travel through normal black paper but electrons are, so to test whether or not electrons or photons are responsible for the enhanced rate seen by the Observer, a black paper was placed between the Emitter and the Observer while measuring the rate of the Observer. Supposing the Emitter generates photons while powered on, the rate should stay at the same level, if the paper is between the two photomultipliers. On the other hand, if electrons are the main cause of the rate increasement the black paper should not make a significant difference with the measurement without the paper. The third scenario would be that electrons and photons are emitted at the same time. That would cause a drop in the observed rate when the paper blocks the photons but will not fall on the ground level due to the number of electrons which will hit the photocathode or the dynodes of the Observer directly.

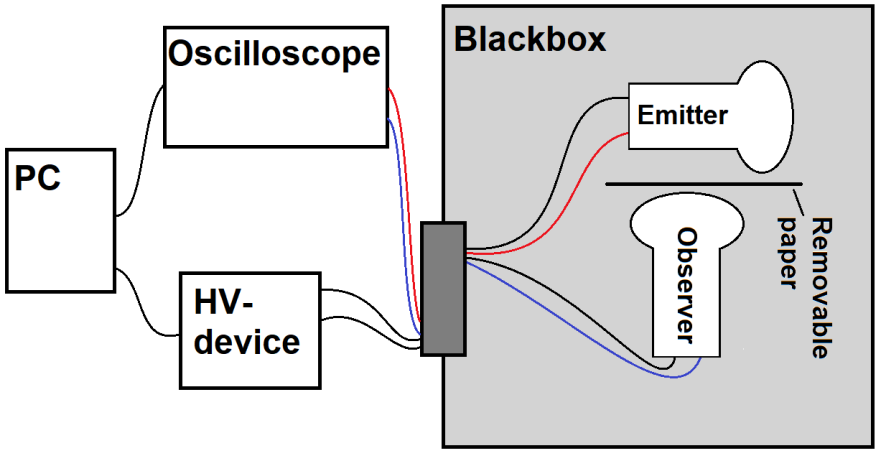

Figure 3.2.2: The measurement setup used to distinguish between electrons and photons. The paper between the photomultipliers can be removed.

The setup used for this measurement is also similar to the first one used, but now a movable paper is built in (see figure 3.2.2). The paper could be moved between the PMTs from outside the dark box with a wire, but not removed again. The execution of for the measurement was the following: First, only the Observer was powered on to measure the dark rate of the Observer for 40 min, then the Emitter was set on 1000 V , to measure the expected increasement of the rate seen by the Observer. After another 40 min, the black paper was put between the two PMTs, to shield the Observer from photons. 40 min after that the Emitter was turned off, the measurement carried on for half an hour. The result of this experiment is shown in figure 3.2.1.

The data shows the expected increasement of the rate of the Observer as soon as the Emitter was powered on. As soon as the paper was moved between the two PMTs the

rate dropped down to the same level than before when the Emitter was off. Also, no difference is visible after turning off the Emitter, still behind the paper. This suggests that the main source which causes the rate increasement are photons, which then get blocked by the paper. It seems that there are no or only a few electrons spawned in the Emitter, otherwise the rate of the Observer would be higher than the dark rate of the Observer with the paper between the PMTs.

3.2.3 Investigation of an insulated PMT

In the paper [31] a PMT was covered with a transparent insulating material to prove that the light emission was generated on the outside of the PMT caused by discharges in the air. With the insulating material on the outside of the PMT, these discharges should be suppressed. The intern explanation for the discharges was, that the dielectric glass is polarized and the electric charges are equally distributed in the glass, sketched on the left side of figure 3.2.3. To get discharges in small gaps of air, for example between the mounting structure and the PMT, the needed voltage on the glass depends on the dielectric constant (κ) which in the case of glass ranges between 5 and 10[1]. Assuming a value of $\kappa = 7.5$ for the glass and a negative fed voltage of 1000 V the outside of the glass should lay on a potential of about 150 V. Discharges could then only be produced between the holding structure and the PMT glass. So if the reason for the emitted photons are discharges on the glass, the insulating lacquer should stop these and the Emitter should not "glow" anymore.

To prove or contradict this hypothesis the experiment was readjusted. The coating material which was used to insulate the PMT is a combination of the insulating lacquer "Electrolube Tropicalising Vanish" and the thinner "Electrolube Universal Acrylic Thinner" with a mixing ratio of one to one. The photocathode of the PMT, as well as the pins on the other side, should not be covered because the insulation lacquer has some wavelength shifting characteristics.During the coating, insulating tape was used to cover

[1]Taken from: http://hyperphysicis.phy-astr.gsu.edu/hbase/tables/diel.html

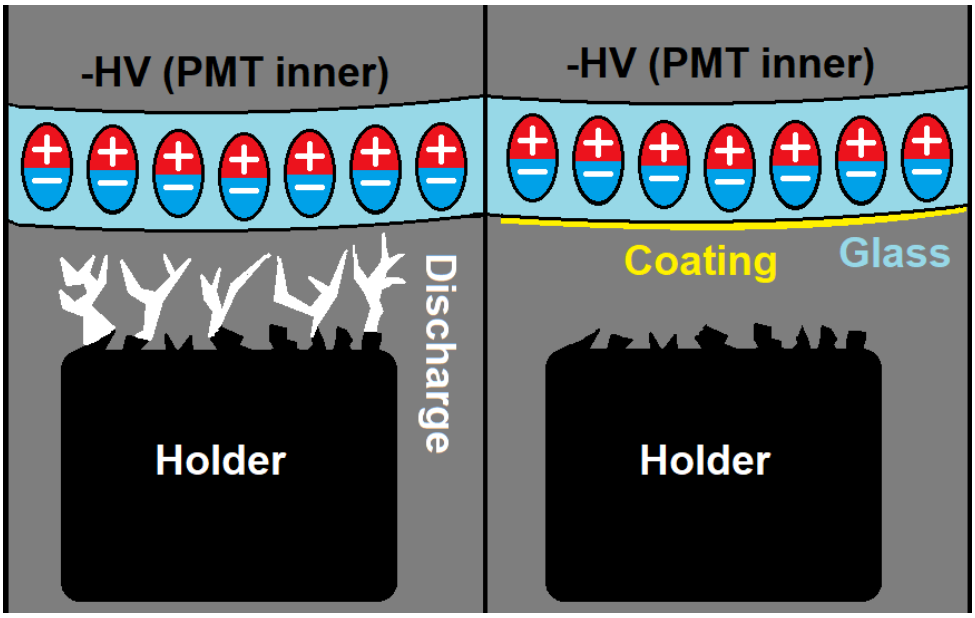

Figure 3.2.3: A rendered picture of the polarization and the discharging (left) and the effect of adding an insulating coating (right).

the photocathode part of the PMT, which was easy to remove after the coating and let no residuals behind. Then the PMT was once dipped completely in the lacquer and the thinner mixture for a few seconds so that everything but the pins was in contact with it. After drying 42 hours the lacquer was hardened and the tape could be removed. It was the first time the working group conducted, this procedure, so the result was not perfect. However, the tube part of the PMT was covered completely and homogeneously without any air bubbles. Nevertheless, the protection of the photocathode part of the PMT was not tight in a few spots and so some residuals of the lacquer were left on the photocathode and the pins. For this work, this should not be a problem because the data from the Emitter PMT is not required in the following experiment.

To see if the insulating lacquer works as expected two measurements were carried out before and after coating the PMT. The first one performed was the same which is described in chapter 3.1.1. In this measurement, the rate of the Observer was measured while the Emitter was turned on and off. If the hypothesis explained before is true, there should be no increasement in the rate of the Observer anymore.

Before the PMT was coated the behavior was like expected (figure 3.2.4) similar to the one seen before in chapter 3.1.1.

The coated PMT showed an interesting behavior in the measurement, shown in figure 3.2.5 , the rate raises at the first and second time the Emitter is on high voltage, but after that, the rate behaves not stable anymore regardless of the applied voltage. In three

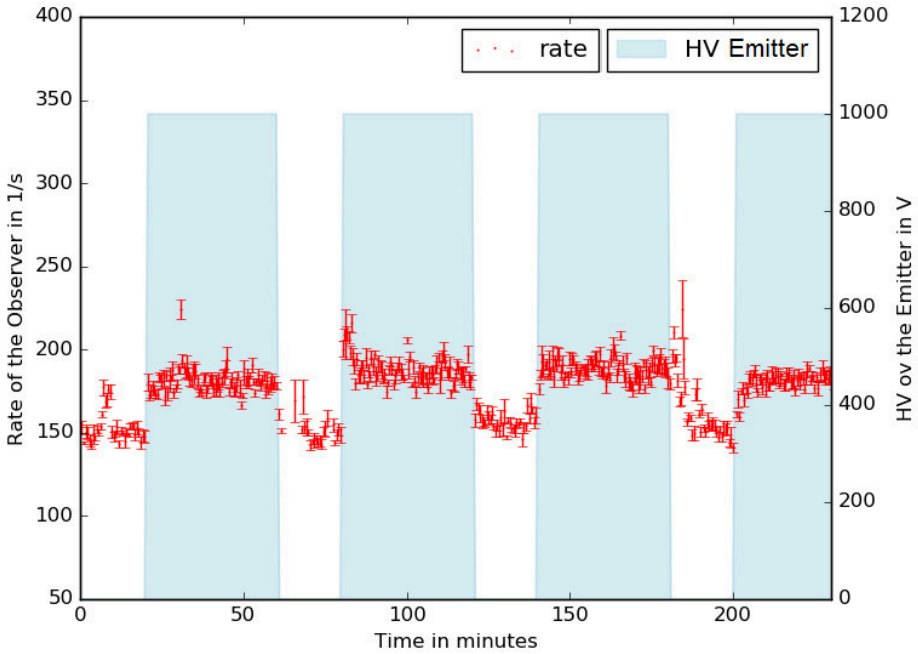

Figure 3.2.4: Measurement of the rate of the Observer facing on the not coated PMT.

measurements this behavior showed up every time after about 120 minutes. This could be explained that something is charging up to a value and then is discharging again in a burst of photons or electrons. To figure out where this unstable rate comes from the base and the pins of the PMT were covered with black neoprene and the measurement was performed again. The data showed that the rate was stable again, shown in 3.2.6. Therefore the unstable rate of the Observer was probably produced in the region of the base and pins of the PMT. During the coating process, some of the lacquer was left behind on the pins, as mentioned before, these residuals could have caused the discharges in the pins. No further investigations into this phenomenon were done. Now comparing the measurements with not coated PMT and with the coated one. In both measurements, the rate raises after powering on the Emitter regardless of the coating. The rate also raises about the same value.

The second measurement done with the coated PMT is the same as the one done in chapter 3.1.1 where the dependence of the supplied voltage of the Emitter on the number of the emitted photons is shown. Figure 3.2.7 displays the result of this measurement. The Observer rate also follows an exponential function as in the earlier measurement. The result of fitting is $(0.91 \pm 0.04) \cdot \exp((4.33 \pm 0.03) \cdot 10^{-3} \cdot x) + (140.41 \pm 0.39)$. The measured rate at 1400 V seems a bit too high. This could have happened because this rate was measured first so the dark rate of the Observer could have been higher than in

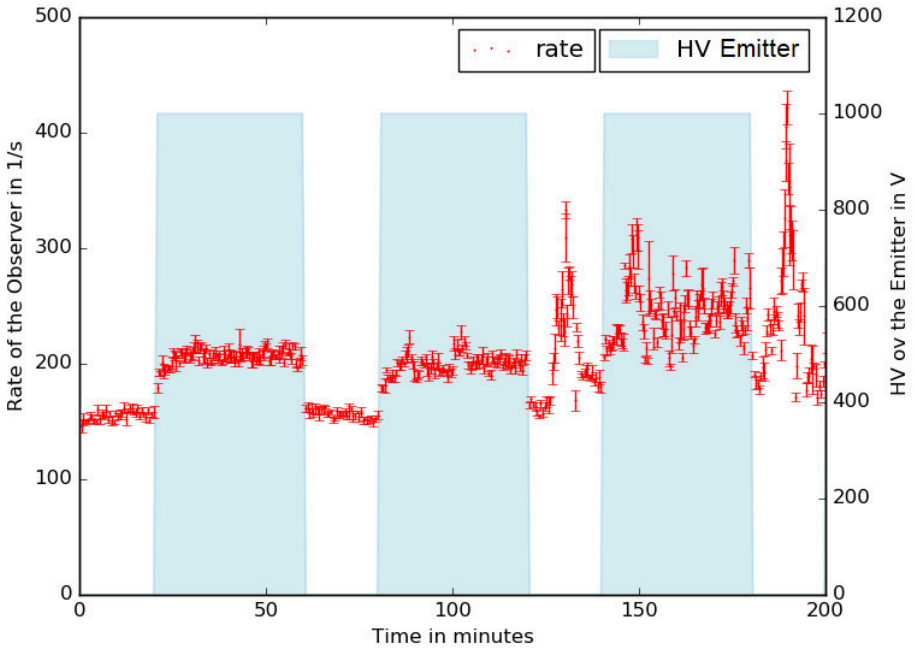

Figure 3.2.5: An example of the not expected unstable rate after 120 minutes of the Observer facing at the coated Emitter.

later measurements of the lower supplied voltages. The exponential factors are similar for both measurements ($b_{coated} = (4.33 \pm 0.03) \cdot 10^{-3}$ and $b_{not\,coated} = (2.56 \pm 0.02) \cdot 10^{-3}$). The multiplication factor of the exponential function of the coated PMT is ~ 7 times smaller than the factor of the not coated PMT shown in chapter 3.1.1. This differences can be explained by the fact that the measured PMT were not the same and not the same one, as mentioned before different photomultipliers only behave similarly and not exactly equal.

The coating of the Emitter PMT did not influence the result of the experiments performed in this chapter compared the results of the previous section. Neither the observed rate nor the exponential behavior of the rate did change with the insulation around the tube of the photomultiplier. These results are contradicting with the results of the KM3Net collaboration [31]. Discharges produced at the glass tube of a photomultiplier are not the reason photons are emitted from a PMT, otherwise, the behavior of the rate independence of the powered or not powered Emitter would have been different, and no or less increasement of the rate would have been measured. The second experiment in this chapter demonstrates as well that the glass tube is probably not the origin of the photons, otherwise, the increase of the number of the emitted photons would have been not that strong.

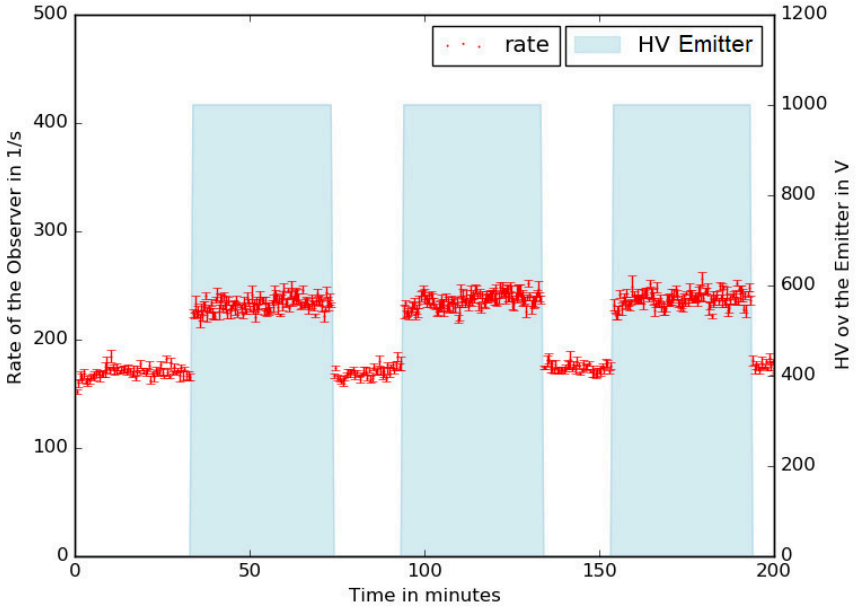

Figure 3.2.6: The measurement of the coated PMT, with the base covered with black neoprene.

3.3 Estimation of emitted photons with a sensitive camera

To define where the photons are generated, the Emitter was photographed with a CCD camera from ANDOR model Newton CCD DU920P Bx-DD. Due to time limitation of two days[2] only a few pictures could be taken without any deeper analysis at that time. Before going into the details of the measurement the working principle and the dark current of a CCD camera will be explained in the following chapter.

3.3.1 Working principle of a CCD camera

Charge Coupled Device (CCD) cameras are fast high sensitive cameras for the spectrum of visible light. The biggest difference to single-lens reflex cameras is, that every arriving photon is transformed into a defined number of electrons by semiconductors. The electrons are stored and counted after a defined period of time. That leads to an image of the light intensity distribution, but without information about wavelength of the incoming

[2]The Camera was of a Spectrograph, which was for testing reasons only available for 2 days.

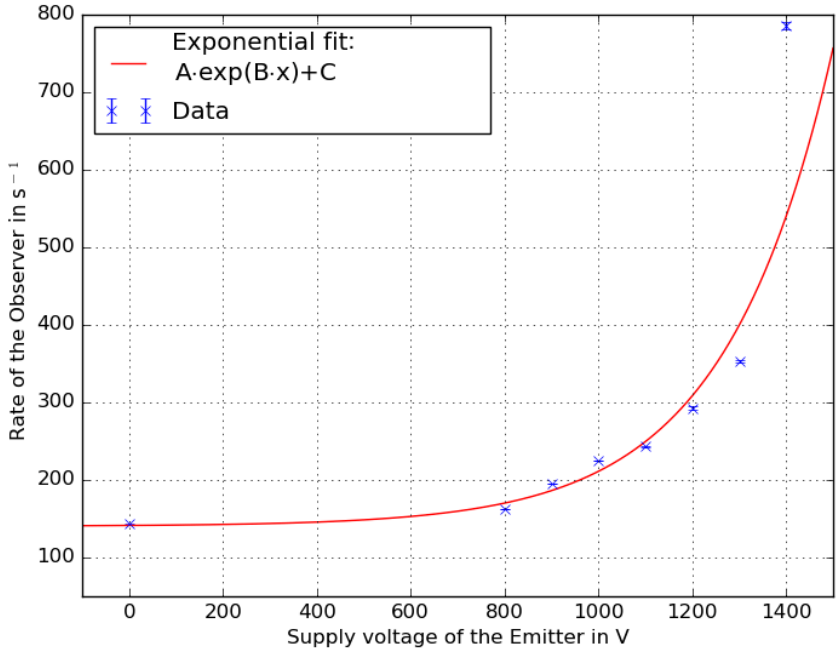

Figure 3.2.7: Measurement rate observed by the Observer plotted against the supply voltage of the coated Emitter.

light[3].

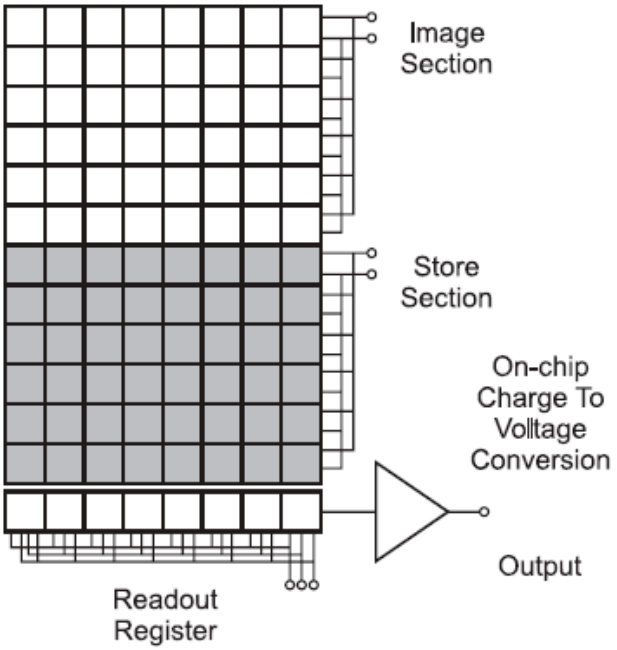

Figure 3.3.1: A sketch of the setup of a CCD camera, with the image section, the store section, and the readout register [32].

The typical CCD camera consists of an image section, a store section, and a readout register as shown in figure 3.3.1. Each pixel collects photons and generates electrons in the imaging section, the electrons are then stored in the store section until the readout mechanism starts. The readout can be done in different ways either each pixel individual, binned in 4 or more pixels or line by line. The images in this thesis were taken, by reading out every pixel which is explained in figure 3.3.2. The bottom row is shifted into the readout register and then pixel by pixel into the readout amplifier, which multiplicates the electrons by a factor which differs for different types of CCD cameras. After saving the number of electrons in the memory, the amplifier is emptied and the next pixel is shifted into the readout amplifier. However, the duration and repetition of the collecting of photons can be freely chosen and after each repetition, the result for every pixel is summed and saved in a data file.

As with a PMT, the CCD camera also features different types of background [32]. There are three different dark currents which will add up to the total noise δ_{total} of a CCD camera and are described as the readout noise $\delta_{readout}$, the dark current δ_{dark}, and the statistical uncertainty of the signal δ_{signal}.

$$\delta_{total} = \sqrt{\delta^2_{readout} + \delta^2_{dark} + \delta^2_{signal}} \tag{3.3.1}$$

The readout noise origins from an intrinsic noise source which generates extra electrons during the amplification process. The dark noise arises from thermally generated charges in the silicon sensor and changes dramatically with the temperature. The statistical uncertainty arises from the external signal. The Poisson statistics gives a noise for a number of incoming photons P which generate N_e electrons in one pixel with quantum

[3]There are also color sensitive CCD cameras, but the one that was used in this thesis was not featuring this.

efficiency D_{QE} and the Signal S as:

$$\delta_{Signal} = \sqrt{S} = \sqrt{D_{QE} \cdot P}. \tag{3.3.2}$$

With the equations 3.3.1 and 3.3.2, the signal to noise ratio can be calculated with

$$\frac{S}{\delta_{total}} = \frac{D_{QE} \cdot P}{\sqrt{\delta^2_{readout} + \delta^2_{dark} + \delta^2_{signal}}}. \tag{3.3.3}$$

3.3.2 Expected background from the CCD camera

The theoretically expected background from the CCD camera will be calculated in this section. Independent of the statistical uncertainty of the signal the used CCD camera has an overall readout noise of 50 kHz and a dark current of 0.0003 electrons per pixel and second. This leads to an uncertainty of 0.21 $\frac{e^-}{\text{pixel}}$ per readout, with five repetitions for an image this leads to 1.04 $\frac{e^-}{\text{pixel}}$. This uncertainty does not account the statistical uncertainty of the signal which is usually greater. In the following calculation of the estimated photons from the photomultiplier, the total noise will be measured and the background will be subtracted from the signal. Thus, the result is free of the dark and readout noise, since the latter it is a camera profile and there should be always the same amount of this kind of noise. Only the statistical uncertainty of the signal changes with the signal but due to

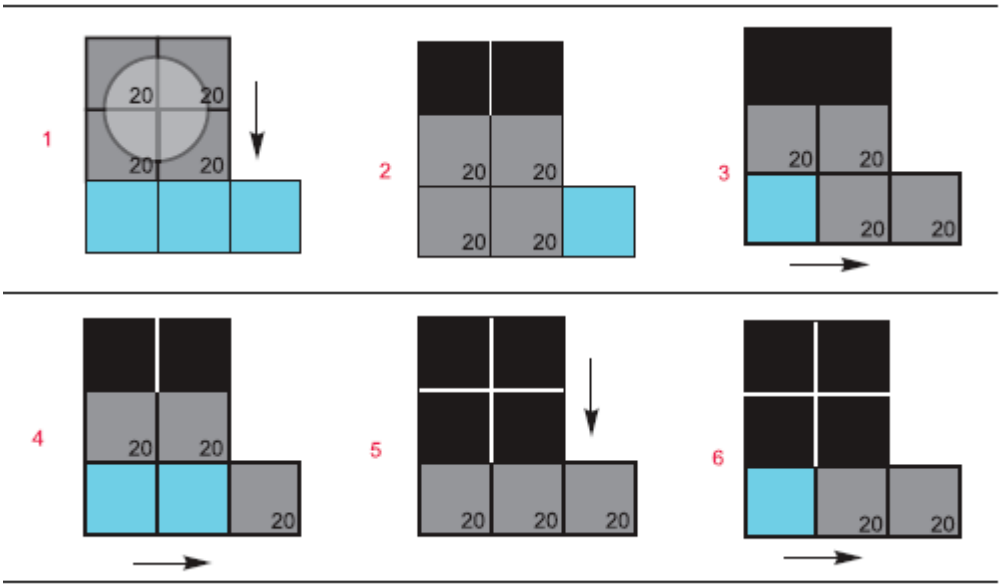

Figure 3.3.2: An example for the readout mechanism of four pixels read out one by one. First, all rows are shifted into the readout register (2) and then shifted one by one into the amplifier (3 & 4) This will continue until all pixels are empty (5 & 6) [32].

the fact that there will be only a tiny difference in the signal, the statistical uncertainty of the signal is also roughly the same. Therefore the internal noise of the camera does not influence the next estimations of chapter 3.3.4.

3.3.3 Measurement results

The CCD camera was not initially planned to be used as a photo camera , however, in two days a few recordings could be managed with the setup showed in figure 3.3.3.

Readout noise per pixel	4 to 8 $e^-/pixel$
Readout noise overall	50 kHz
Dark current	0.003 $e^-/pixel \cdot s$
Preamplifier gain	×4
Resolution	1024 × 255
Pixel size	(24 × 24) μm
Image area	(26.7 × 6.7) mm
Cooling temperature	−80 °C

Table 3.3.1: Camera specifications

The working group was testing a spectroscope where the CCD camera was mounted on. So the camera had no lens to focus on objects. A workaround for that was acamera lens from Canon model EF-S 60mm f/2.8 Macro which was placed directly in front of the camera to get sharp pictures. Between the camera lens and the PMT was 15 cm. An alpha source was placed in front of the PMT, and the supply voltage of the PMT was set to 1200 V to improve the number of emitted photons.

The idea of these photographs was to actually see the emitted photons from the dyn-

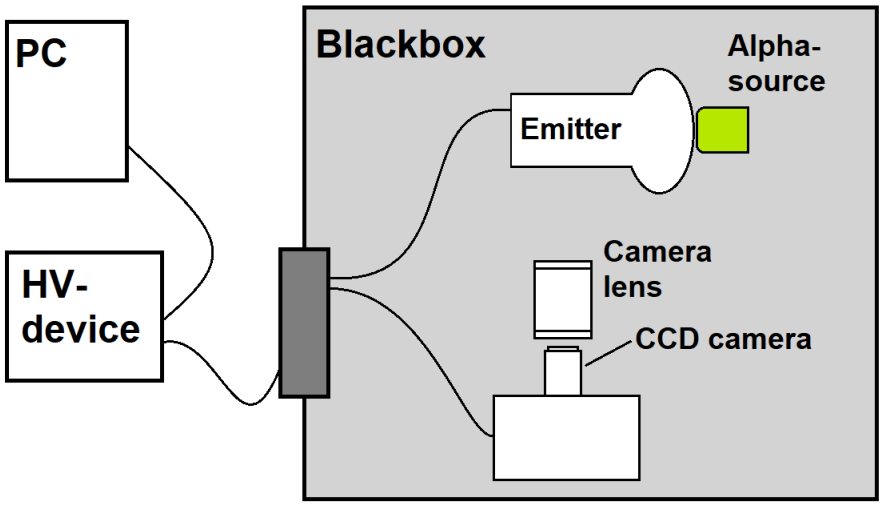

Figure 3.3.3: The setup which was used to take the images of the PMT with the CCD camera.

ode structure as an increased light intensity in some regions. As well as to calculate how many photons were produced. Therefore the focus of the camera was fixed on the dynode structure where the origin of the photons was suspected to be. This thesis will focus on one set of photos, one picture was taken from the not powered PMT as a background reference and from the PMT on high voltage as the signal. Each picture was taken with an integration time of 60 seconds and a repetition of 5 times. After each integration, the software provided by ANDOR compared the just taken integration with the previous one to remove unstable light effects like muons traveling through the image or the store section which produced extra light or electrons. This software could have also removed some sparks or other unlocalized lightning effects from the PMT like air discharges, which was not taken into to account during the two days of recording and could not be turned off afterward due to the time limitation.

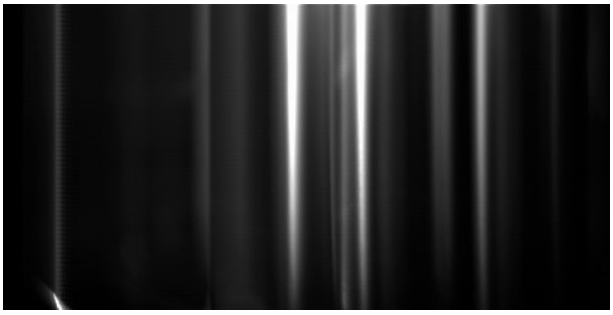

Figure 3.3.4: A picture of the dynode structure, taken with the CCD camera while the light was switched on.

The image of the dynode structure was covering a similar sector as shown in figure 3.3.4, with and without an applied voltage of 1200 V to the PMT. As visible in figure 3.3.5, where the Emitter was not powered on, the dark box is not perfectly dark and therefore some reflections are visible. An explanation for the light inside the dark box is the power adapter of the spectroscope, which had to be placed inside the blackbox

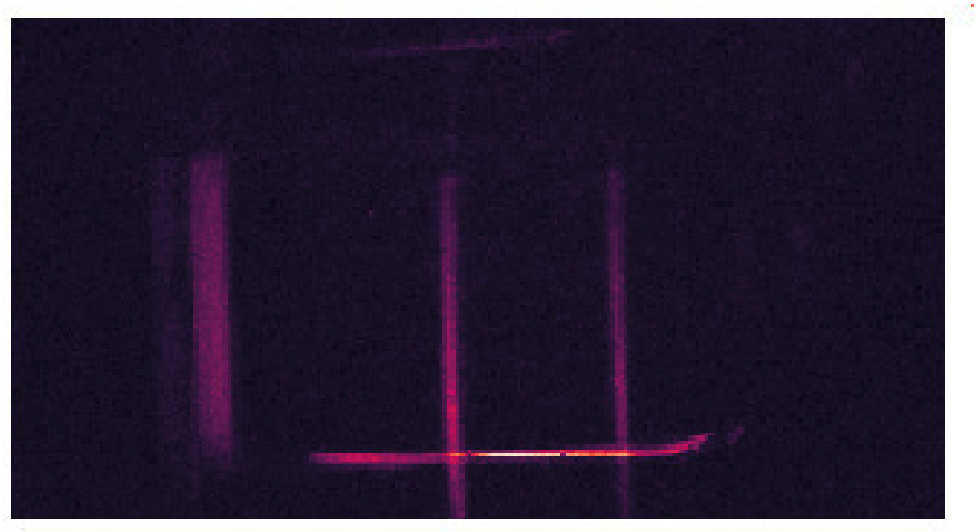

Figure 3.3.5: The light intensity of the dynode structure, measured with the CCD camera. The bright parts are areas of reflected light.

cause to a too short cable. This power adapter had a bright LED built inside which could not be completely covered since it would have prevented a proper heat dissipation of the device. The taken reference background will help to localize the reflection areas which then will not be taken into account when the emitted photons are calculated in the next chapter. The "background" image was subtracted from the "signal" image both taken from the same perspective. The resulting, now called subtraction image should show the additional light from the Emitter, it is shown in figure 3.3.6 with the green areas of the reflected light. There is no showy lightened part of the image, so no strong glowing dynodes are leaping out. Also, the few barely visible points which are noticeable in the signal image can be found in the background image. So with this method, the origin could not be located inside the PMT. With more time and more careful investigations, it may have been achieved.

3.3.4 Estimation of the number of emitted photons

The images taken above are still useful to estimate the number of emitted photons from the Emitter which could not be detected by the CCD camera. To do that the needed information of the camera is listed in table 3.3.1. Considering that the light could be emitted from the dynode structure and also from the glass tube. The part of the

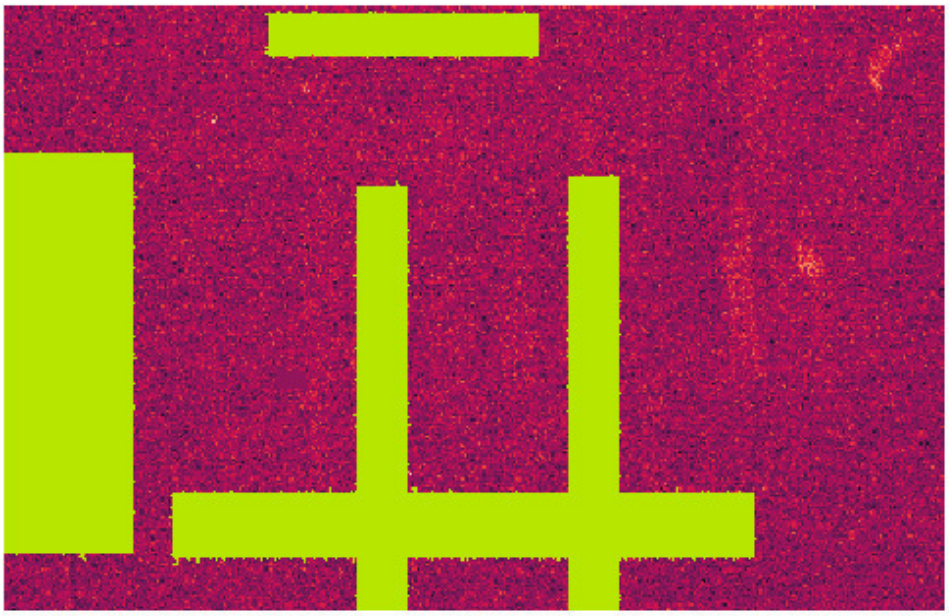

Figure 3.3.6: The subtraction image (background image subtracted from the signal image). The green parts are the areas of reflected light which are not taken into account for the calculation of the mean intensity signal.

measured glass tube can be calculated: Therefore the length of the dynodes, as well as the diameter of the PMT, were measured to calculate the surface of the glass that is covered in the image. The measured length of the dynode structure is $l_D = (25.0 \pm 2.0)$ mm, the diameter of the PMT is $d_C = (52.5 \pm 1.0)$ mm, so the opening angle θ of the camera can be calculated over

$$\begin{array}{rrcl} & \sin(\frac{1}{2}\theta) & = & \frac{l_D}{d} \\ \Leftrightarrow & \theta & = & 2 \cdot \arcsin(\frac{l_D}{d_C}) \\ \Leftrightarrow & \theta & = & (56.87 \pm 0.46)\,^\circ \end{array} \tag{3.3.4}$$

With this angle, which is $p = (15.79 \pm 4.61)$ % of a whole circle, the size of the surface of the depicted part of the glass U_{Glass} can be calculated with the formula for the circle times the height of the glass cylinder $h_C = (50 \pm 2)$ mm and with the height of the dynode structure $h_D = (26 \pm 2)$ mm.

$$\begin{array}{rcl} U_{Cylinder} & = & \pi \cdot d_C \cdot h_C \\ & = & (8246.88 \pm 72.5)\ \text{mm}^2 \end{array} \tag{3.3.5}$$

$$\begin{array}{rcl} U_{glass} & = & U_{Cylinder} \cdot \frac{d_D}{h_C} \cdot p \\ & = & (677 \pm 6)\ \text{m}m^2 \\ & \hat{=} & (8.21 \pm 0.07)\ \% \end{array} \tag{3.3.6}$$

It turned out that the part of the glass tube on the images represents (8.21 ± 0.07) % of the whole tube. When only considering the dynode structure the calculation is simple, the image shows only one side of the dynode cube inside the PMT with the three lengths of $a = b = (25 \pm 2)$ mm and $c = (26 \pm 1)$ mm so (16.88 ± 4.63) % of the dynode structure is covered on the image.

Assuming that no light gets absorbed in the camera objective, the photons emitted by the PMT can be estimated. Therefore the mean intensity $\bar{x}$ of the subtraction image was calculated with the Gaussian distribution by:

$$\bar{x} = \frac{1}{n} \sum_i x_i \ ,$$

where x_i is the number of electrons collected by pixel i and n is the number of pixels. With the equation

$$\Delta x = \sqrt{\frac{1}{n-1} \sum_i (x_i - \bar{x})^2}$$

the standard deviation Δx is calculated.

The dynode structure does not fill the whole image, it only extends over 400 rows in the middle that means between the 350th and the 750th row. To calculate the mean value and the uncertainty from the subtraction image the areas of reflection highlighted in figure 3.3.6 are excluded. In this regions, the light intensity is not stable and it would falsify the

result of the estimation for the upper limit of emitted photons. For the leftover area the mean value was calculated as $\bar{x} = 1.45 \frac{e^-}{\text{pixel}}$ and a standard deviation of $\Delta\bar{x} = 4.86 \frac{e^-}{\text{pixel}}$.

With this mean value, the estimation of the emitted photons can be done. Considering that there are (400×255) pixel $= 102000$ pixel in the image (147707 ± 179177) e^- were detected overall. Each detected photon leads to four electrons due to the pre-amplifier gain of the CCD camera, so the number of detected photons overall is (36927 ± 46180) γ. This number of photons is the estimation for the viewed part of the photomultiplier, with the percentage calculated above (eq. 3.3.6) the number of photons emitted by the whole PMT from the glass or from the dynode structure can be calculated. If the light only gets emitted by the glass tube of the PMT the upper limit is (463688 ± 562482) γ, and if only the dynode structure is the origin 218760 ± 273576 photons were emitted at the most.

The big uncertainty is caused by the fluctuations in the subtraction image. It could have been removed by placing the PMT and the camera in a blackbox wich is totally light tight and measuring with longer integration time. With such a big uncertainty the measurement does not provide a credible answer if photons were detected or not. The calculated upper limit with lower uncertainties should have been seen on the taken image of the CCD camera and would also lead to a higher rate seen by the PMT, in other measurements.

The observed increasement of the rate seen before in chapters 3.1.1 at 1400 V was about (200 ± 15) s^{-1}. To calculate how many electrons the CCD camera would have been measured, the number of photons measured with the PMT can be transmitted into electrons which should have been seen by the camera. Over the same period of time of five times 60 seconds integration, the PMT collected 60000 ± 245 photons. Concerning the camera would take an image with the same amount of pixels than before, the area of the imaging section of the PMT has also be taken into account. A rough estimation leads to the assumption that the Observer was able to cover 25 % of the dynode structure. The camera, which sees less of the PMT, would just collect

$$\frac{8.31\,\%}{25\,\%} \cdot 60000\,\text{photons} = (19944 \pm 142)\ \text{photons}.$$

The images taken by the CCD camera was taken with a Canon EF-S 60mm f/2.8 Macro camera lens which has a smaller aperture opening than the PMT without a pinhole. To take this into account the area of the smallest pinhole of the lens system was compared to the area of the PMT photocathode, which leads to a factor of

$$\frac{A_{lens}}{A_{PMT}} = \frac{8.04\,\text{cm}^2}{40.72\,\text{cm}^2} = 0.20.$$

After multiplying this factor to the previouse calculation, (3989 ± 64) photons would contribute to the image. Compared to the observed photons from the measurement this number seems very low. An Explanation for that is the divergent Quantum efficiencies (QE) as shown in figure 3.3.7.

The QE of the camera has its maximum at a wavelength of 700 nm to 800 nm where the PMT is not sensitive anymore. The PMT was developed to detect light in the visible range, so the QE has its maximum around 400 nm and is blind to the light of wavelength smaller than 300 nm and longer than 650 nm. Since in the QE range of the PMT, the CCD camera has similar efficiencies the additional light seen by the camera could be lower energetic photons which the PMT could not detect. The QE in the region of the PMT does not influence the number of photons which shout be at least seen by the CCD camera.

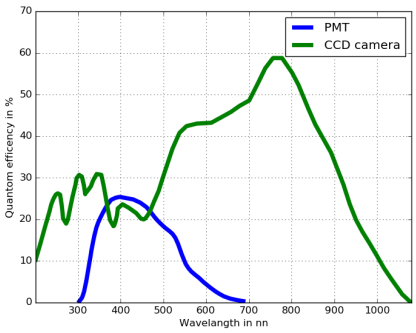

Figure 3.3.7: Comparison of the QE of the CCD camera and the PMT [33, 23].

The final question of this chapter is if the camera should have measured a significant increased signal in locations where the light is generated in the dynode structure. For that, the statistical uncertainty of the signal of the expected photons calculated from the rate seen by the PMT is compared with the background noise calculated in chapter 3.3.2. For this composition the calculated photons, in the wavelength rannge of the PMT, have to be converted into electrons by multiplying them with the pre-amplifier gain of the CCD camera

$$(3989 \pm 64)\ \text{photons} \cdot 4\,\frac{\text{electrons}}{\text{photons}} = (15956 \pm 127)\ \text{electrons}.$$

The statistical uncertainty of the signal is the total amount of by the square root of the calculated electrons, which leads to a statistical uncertainty of the signal of $\sqrt{15956}\,\text{electrons} = 127\,\text{electrons}$ for all pixels together.

Compared to the noise of the CCD camera calculated in chapter 3.3.2 of $1.04\,\frac{\text{e}^-}{\text{pixel}}$ which leads to 106080 electrons for the whole image, the signal detected by the PMT could not be distinguished.Unfortunately, the actual dark current of the CCD camera was not measured, due to the limitations of time.

The calculated result of 106080 electrons needed to be greater than the statistical uncertainty appears rather dramatically high but taking into account that the dynode structure would only glow in small parts of the taken picture, only a few pixels would be illuminated and therefore the CCD camera should be able to detect these photons. With more time better results could have been achieved with this setup and the origin of the photons may have been located, with longer measurements and better preparation.

3.4 Timing and number of emitted photons

After proving the emission of photons from the Emitter, information about the photon properties are needed, to detect the origin of these photons. For that reason, the measurements in this chapter will care about the timing and the number of the emitted photons. The timing will describe the arriving time of the generated photons by the Emitter, in respect to the trigger signal of the LED pulser. From the number of emitted photons measured via the amplitude of the PMT signals, one can tell if only single photons or bursts are emitted from the PMT.

3.4.1 Timing of the emitted photons

To estimate where the photons are generated inside the PMT, the arriving time of the photons will be investigated in this chapter. For the measurement, the Emitter will be trigged with light from a LED pulser. The Observer is facing the dynode structure of the Emitter and shielded against the light of the LED pulser. This setup is shown as a sketch in figure 3.4.1. The time difference between the starting point, defined by the signal of the LED pulser, and the time of a pulse from the Observer is called arriving time of the photon. A pulse of the Observer is defined by a value of 2 mV (0.25 phe), every time this threshold is passed the arriving time is saved. This measurement was done two times: One time with the powered Emitter, and one time with the not powered Emitter in front of the Observer. The measured times will then be presented as a histogram. The expected result of this measurement is, to see either an extra maximum in the histogram or just a homogeneous increasement of the pulses which arrive later than the expected main pulse. The expected main pulse will describe the arriving time of the reflected light from the LED pulser. By calculating the time difference between the additional peak to the main peak the origin of the photons can be estimated.

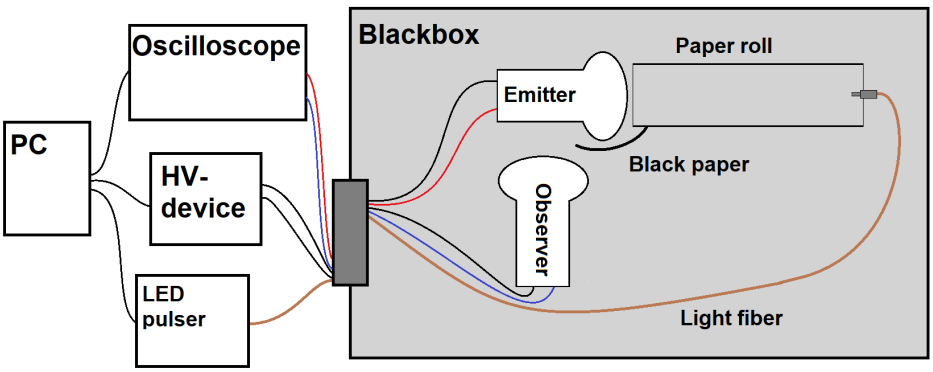

Figure 3.4.1: Setup for the timing measurement. The brown line represents the light fiber, and the Observer is shielded against the light from the LED.

In figure 3.4.2 the taken data is shown. On the x-axis, the arriving time is written. The zero mark is lined up with the explained main peak, corresponding to the reflected light of the LED. The y-axis corresponds to the counted pulses. The blue bars are representing the data taken by the Observer while the Emitter was powered and the green bars while the Emitter was off.

The measured number of data points for both measurements were the same, so it can be compared. The reflection peak of both measurements matches as expected. In the blue data where the Emitter was powered on additional peak appears (3 ± 1) ns after the main peak, this peak represents the photons which were emitted from the Emitter. A second small extra peak is noticeable (6 ± 1) ns after the main peak.

With this numbers and the knowledge of the inner structure and about the voltage distribution of the dynodes inside the PMT, the distance, an electron could travel in this time, can be calculated approximately with the law of the energy conservation. The approximation for the velocity of the electron $v_{e^-} = \frac{s}{t}$ was also done, with s for the distance and t for the travel time. The distance is calculated in equation 3.4.1,

$$\begin{aligned} E_{kin} &= \tfrac{1}{2} m_{e^-} v_{e^-}^2 &&= Ue \\ \Rightarrow \quad v_{e^-} &= \sqrt{\tfrac{2 \cdot U \cdot e}{m_{e^-}}} \\ \Rightarrow \quad s &= \sqrt{\tfrac{2 \cdot U \cdot e}{m_{e^-}}} \cdot t \end{aligned} \tag{3.4.1}$$

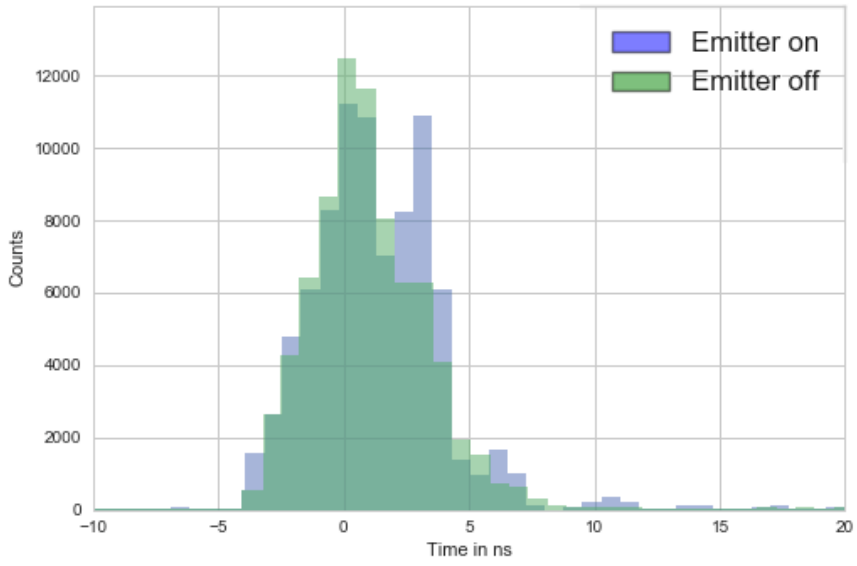

Figure 3.4.2: Results of the timing measurement, the counts of the pulses are plotted against the arriving times. In blue the taken data for the powered Emitter, in green for the not powered Emitter.

where $m_{e^-} = 9.11 \cdot 10^{-31}\,\text{kg}$ is the mass of the electron and $e = 1.602 \cdot 10^{-19}\,\text{C}$ is the charge of an electron. The voltage U between the cathode and the first dynode[4] is $\frac{4}{13}$ of the supplied voltage of the PMT[5], so $U = \frac{4}{13} \cdot 1000\,\text{V} = 230.7\,\text{V}$. For the measured time of $t_1 = (3 \pm 1)$ ns this leads to a traveled distance of $s_1 = (27.0 \pm 9.1)$ mm, and for the time of the second pulse $t_2 = (6 \pm 1)$ ns a distance of $s_2 = (54.1 \pm 9.1)$ mm.

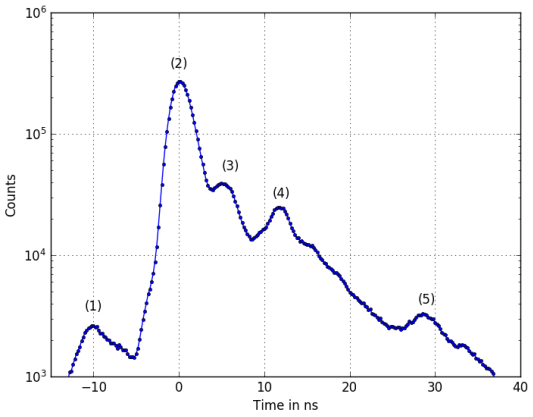

Figure 3.4.3: Measurement of the timing of the PMT signals [34], done with an HQEHA BA301 from Hamamatsu. Marked are the different peaks caused by the correlated background (1,4,5), the peak of seen light (2), and the peak caused by light from the first dynode (4).

Considering the real spacing of the photocathode and the first dynode is (53 ± 5) mm and the first and second dynode have a spacing of $18 \pm 3\,\text{mm}$[6]. The time which corresponds to this distance of the photocathode and the first dynode, calculated with the rearranged equation 3.4.1 is (5.9 ± 0.8) ns. On the first view, the calculated traveled distance of the electrons of $s_1 = (27.0 \pm 9.1)$ mm and the measured spacing between the dynodes does not fit. But, because of the greatly simplified calculation of the traveled distance of the electron, without taking the acceleration of the electron, and the voltage of the other dynodes into account, it is legitimate to formulate the hypothesis that the first peak corresponds to photons emitted of the first dynode and the second peak to photons generated by the second dynode. The size of the second peak can also be explained by this hypothesis. The energy of the secondary electrons is bigger when hitting the first dynode, due to the longer acceleration way and the greater voltage gradient, so the probability to generate photons is higher on the first dynode than on the second.

Another hint that this hypothesis is true provides a measurement by Markus Dittmar in his bachelor thesis [34]. The PMT HQEHA BA301 was developed in characterized. The mentioned measurement is shown in figure 3.4.3, the timing of the pulses from the studied photomultiplier was measured similar to the last measurement, but this time it the pulses are only from the PMT itself. Again the number of the pulses are plotted against the time and the origin of the coordinate system corresponds to the time of the main pulse (2). The correlated background which was explained in chapter 1.2.2.3 is also visible in this measurement. Peak number (1) represents the pre-pulses, the peaks (4) and (5) are

[4]This was chosen because the distance between the photocathode and the first dynode is the longest and it is expected that the electron travels only this distance.

[5]Taken from: https://www.hamamatsu.com/resources/pdf/etd/R12199_TPMH1356E.pdf

[6]The relative big uncertainties result of the curved form of the dynodes.

caused by the afterpulsing. The only pulse which cannot be explained by the correlated background is the pulse marked with (2). This peak appears $\sim 5\,\text{ns}$ after the main pulse. Even though this measurement is from another PMT as the one which is studied in this thesis, it has the same size and roughly the same spacing between the dynodes. Due to that fact, the time of 5 ns is comparable with the calculation done before. This would also lead to the conclusion, that photons are emitted from the first dynode.

If the photons are produced on the first dynode, they should be visible, if the Observer faces directly on the first dynode of the Emitter. That means that the photocathodes of both PMTs are facing towards each other. The Emitter PMT is stimulated with a light signal via a glass fiber. To get as low reflection as possible the end of the glass fiber is directly connected to the photocathode of the Emitter and the intensity of the light pulses are very low. The first measurement was done with the Emitter on negative and the Observer on positive high voltage, as in the measurements before. This setup caused an unstable rate from the Observer, as shown in figure 3.4.4. A possible reason for this behavior is that the gradient between the photocathode of the Observer and the Emitter was too high and the Observer was not working correctly due to the influence of the high voltage near the grounded photocathode. A second measurement with a negative supply voltage on the Observer was performed, the taken data is shown in figure 3.4.5b. The rate of the now on negative high voltage operating Observer is stable and in comparison to the former measurements quite high. The rate raised $300\,\frac{1}{\text{s}}$ which is an increasement of almost 400 % compared with former measurements. This result supports the theory that the first dynode is the main source of the emitted photons.

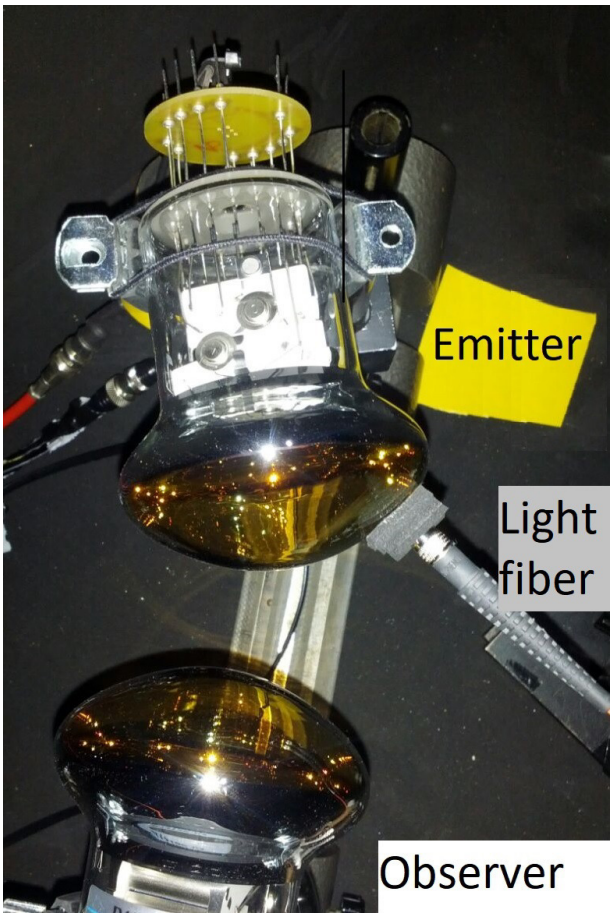

Figure 3.4.4: Real setup of the measurement of the first dynode.

The measurements in this chapter have shown that the best candidate for the emission of the photons is the first and largest dynode of a photomultiplier. The results from the timing experiment and from the bachelor thesis by M. Dittmer have also strong arguments for this theory. The additional dynodes are contributing a little bit to this emission, but

the prominent part is coming from the first dynode. Another interesting conclusion of this measurement is the bad influence of strong electric field near the photocathode of a PMT unless the cathode of and the electric field are from the same level and strength. In the mDOM, this is not a problem because the photomultipliers are all powered with the same polarization and the photocathodes are directly facing at each other.

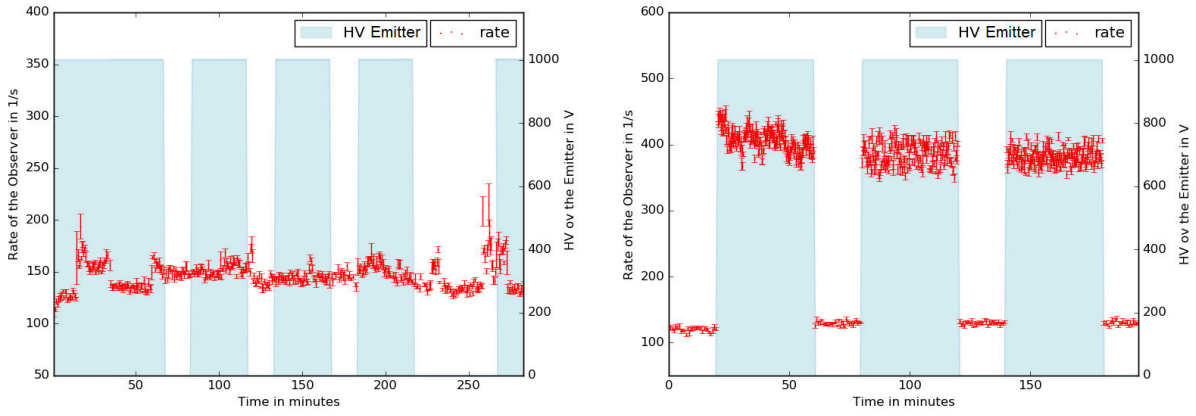

(a) (b)

Figure 3.4.5: Left: First measurement of the rate of the Observer, facing onto the first dynode of the Emitter. The Observer is on positive and the Emitter on negative high voltage. The voltage gradient causes the unstable rate.
Right: Second measurement with the Observer on negative high voltage.

3.5 Number of emitted photons

With the same setup as presented in figure 3.4.1 the number of emitted photons was measured. The oscilloscope was triggered by the signal of the LED pulser and measuring the amplitude of the pulses which the Observer produced in a defined time window. The measurement was performed two times: one's time with the powered Emitter and one time with a not powered Emitter. By comparing the background measurement, taken only from the working Observer, with the signal measurement, taken from the Observer in front of the powered Emitter, the number of emitted photons by the Emitter can be distinguished. The spectrum will be dominated by the photons from the reflection light from the LED pulser, but there should also be a small difference between the measurements which corresponds to the extra photons emitted from the Emitter.

In figure 3.5.1 the taken data is shown. The green data shows the value of the amplitude of the Observer signal with the not powered Emitter and in blue the data from the Observer in front of the powered Emitter. On the x-axis the height of the amplitude in mV is potted and the number of data points for each amplitude is counted in the y-axis. The second x-axis represents the photoelectrons, corresponding to the calculated trigger level in chapter 2.2. For both measurements, 250000 data points were saved to

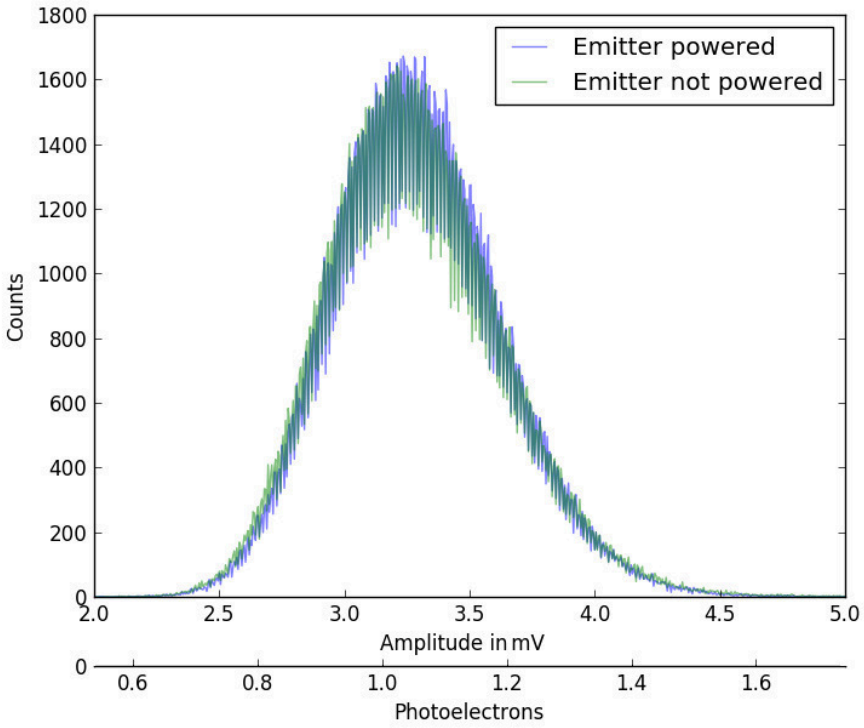

Figure 3.5.1: Data of the amplitude measurement, measured by the Observer.

get comparable results. Both peaks are located around 1 phe which means the Observer detected most of the time single photons, from the LED pulser.

The difference between the two measurements become visible, by subtracting the data where the Emitter was turned off (background) from the data when the Emitter was powered on (signal). Figure 3.5.2 shows the resulting distribution. In the data, two peaks are recognizable one in the negative around 0.9 phe and one in the positive, around 1.1 phe. This shows the shift to higher amplitudes, so to more photoelectrons overall, when the Emitter is turned on. The number of more detected photons is small but still significant, as the uncertainty ΔA for each detected amplitude has the maximum at $\Delta A = \sqrt{1672} = 40.8$ which is lower than the calculated differences in figure 3.5.2. The amplitude of the pulses the Observer detected was only measured in a small time window where the photons of the first dynode were suspected. The low number of extra detected photons can be explained with this restriction. However, the Observer detected in average increasement of the emitted photons by roughly 0.2 .phe when the Emitter was powered.

This result shows that the emitted photons from the first dynode of the PMT are mostly single photons. So they are probably not produced via discharges but by relaxation effects of excited atoms.

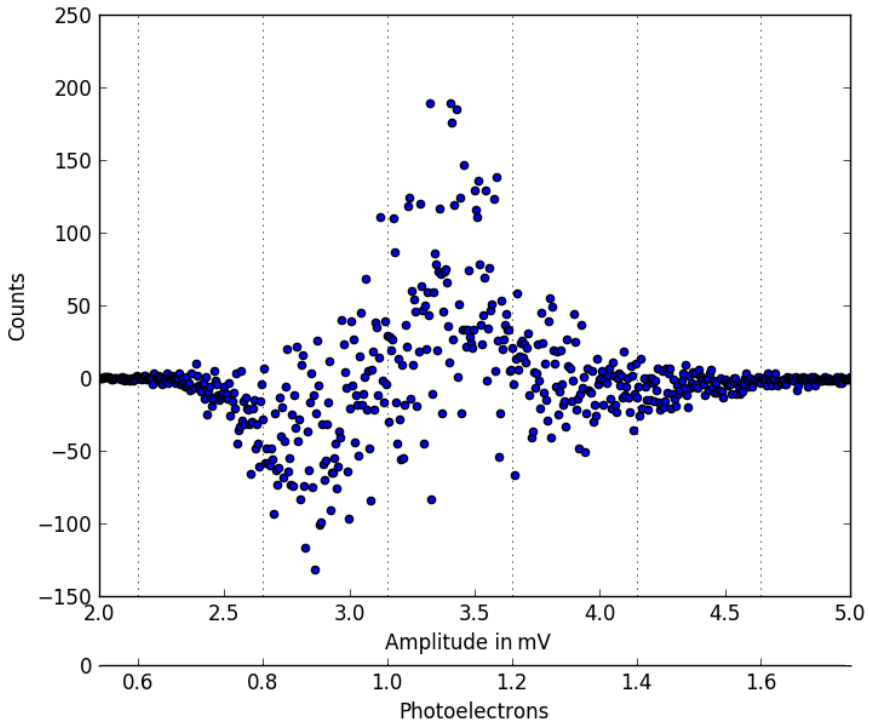

Figure 3.5.2: The comparison between the counts of each amplitude by subtracting the background (Emitter off) from the signal (Emitter on) measured by the Observer.

Chapter 4

The resume and the future

The goal of this work was to investigate the background light sources in a photomultiplier operated at negative high voltage for the development of the multi photomultiplier digital optical module. The first step was to measure the behavior of the rate of a photomultiplier when facing the glass tube and the dynode structure of another PMT. As expected and measured by other collaborations before, the observed rate increased when powering the Emitter PMT [31, 29, 30](chapter 3.1.1). The next question was: Why dose the rate go up and what causes this increasement? The theory that photons are emitted by the PMT was tested and proven, by placing a paper between the PMTs which should only block photons, but not electrons or an electromagnetic field (chapter 3.2.2). With the black coated PMT by Hamamatsu is was clarified that the photons are in fact originate from the photomultiplier is self and were not generated by the pins or the base (chapter 3.2.1). The idea discharges on the glass are causing the emission of photons was refuted by measuring a photomultiplier coated with an insulating but transparent lacquer (chapter 3.2.3).

To locate the source of the emitted photons images were taken with a CCD camera, unfortunately this could not be measured (chapter 3.3). But with the result of the next part where the location of the photons source was estimated via the timing of the incoming pulses from the Emitter, it can be explained. The result was that the first dynode, which is also the largest dynode of the PMT emits the most observed photons. The studied image taken with the CCD camera was only taken from dynodes in the middle of the PMT and not from the first dynode. With more time to use the CCD camera, the first dynode could have been measured, but this was not known while the time of measuring. The timing measurement (chapter 3.4) showed that the best guess where the photons are produced is the first dynode and only single photons are emitted. By photographing the first dynode of the PMT these emitted photons should become visible.

The results of this work do not imperil the mDOM, developed in the group in Münster. The dark rate of the photomultiplieres inside the mDOM will not be influenced by the effect of emitted photons from a PMT. Because all PMTs wich are used will have the coating provided by Hamamatsu measured in chapter 3.2.1 where no emission was measured at all.

In future investigations on this topic the energy could be measured with the help of colored filters which cover only a small wavelength range. With the measured energy of the photons the production process or the material which emits the photons could be investigated. The position of the photon origin could be also studied by measuring the PMT with a raster of a few millimeters.

Bibliography

[1] M. Herrero. The standard model. In T. Ferbel, editor, *Techniques and Concepts of High Energy Physics X*, pages 1–59. Springer Netherlands, 1999.

[2] E. K. Akhmedov, A. Dighe, P. Lipari, and A. Y. Smirnov. Atmospheric neutrinos at super-kamiokande and parametric resonance in neutrino oscillations. *Nucl. Phys. B542*, 1999.

[3] Peter W. Higgs. Broken symmetries and the masses of gauge bosons. *Phys. Rev. Lett. 13, 508*, 31.08. 1964.

[4] E. Resconi T. K. Gaisser, R. Engel. *Cosmic Rays and Particle Physics*. Cambridge University Press, 2016.

[5] et al. (Particle Data Group Collaboration) K. A. Olive. eview of particle physics. *Chin. Phys. C38 (2014) 090001*, 2014.

[6] C. G. S. Costa. The promt lepton cookbook. *Astropart. Phys. 16 (2001) 193-204 Preprint arXiv:hep-ph/0010306*, 2001.

[7] J. K. Becker. High-energy neutrinos in the context of multimessenger astrophysics. *Phys. Rep. 458 (4-5) (2008) 173 - 246*, 2008.

[8] Dr. Lew Classen. *The mDOM - a multi-PMT digital optical module for the IceCube-Gen2 neutrino telescope*. PhD thesis, Friedrich-Alexander-Universitaet Erlangen-Nuernberg, 2017.

[9] Pierre Auger Collaboration. The pierre auger cosmic ray observatory. *Nucl. Inst. Meth. A 798 (2015) 172 - 213.*, 2015.

[10] F. Aharonian at al. The h.e.s.s survey of the inner galaxy in very high energy gamma rays. *The Anerican Astrinomical Society*, 2006.

[11] E. Fermi. Versuch einer theorie der beta-strahlen. *Zeitschirft für Physik 88 (1934) 3-4.*, 1934.

[12] et al. G. Drexlin. Current direct neutrino mass experiments. *Advances in High Energy Physics 2013*, 2013.

[13] K. Greisen. End to the cosmic-ray spectrum? *Phys. Rev. Lett. 16 (1966) 748-750*, 1966.

[14] G. T. Zatsepin and V. A. Kuz'min. Upper limit of the spectrum of cosmic rays. *Soviet Journal of Experimental and Theoretical Physics Letters 4 (1966) 78.*, 1966.

[15] V. S. Berezinskii and G. T. Zatsepin. Cosmic neutrinos of superhigh energy. *Yadern. Fiz. 11 (1970) 200*, 1970.

[16] P. A. Čerenkov. Visible radiation produced by electrons moving in a medium with velocities exceeding that of light. *Physical Review*, 52(4):378–379, aug 1937.

[17] et al. (IceCube Collaboration) M. Aartsen. Neutrino observatory: Instrumentation and online systems. *Preprint arXiv:1612.05093 (2016).*, 2016.

[18] et al. (IceCube Collaboration) M. Aartsen. Icecube-gen2: A vision for the future of neutrino astronomy in antarctica. *Preprint arXiv:1412.5106*, 2014.

[19] et all (IceCube-Gen2 Collaboration) L. Lu. A dual-pmt optical module (d-egg) for icecube-gen2. *PoS ICRC2015 (2016) 1137*, 2016.

[20] et al. (IceCube-Gen2 Collaboration) D. Hebecker. Progress on the development of a wavelength-shifting optical module. *PoS ICRC2015 (2016) 1134*, 2016.

[21] Martin Antonio Unland Elorrieta. Studies on dark rates induced by radioactive decays of the multi-pmt digital optical module for future icecube extentions. Master's thesis, Westfaehlische Wilhelms-Universitaet Muenster, 2017.

[22] S.-O. Flyckt and C. Marmonier. *Photomultiplier Tubes Principles and Applications*. Photonis, Brive, 2002.

[23] Raffaela Solveig Busse. Setup and commissioning of a test stand for detailed investigations of quantum efficiency characteristics of photomultiplier tubes, and initial studues for icecube-gen2. Master's thesis, Westfaehlische Wilhelms-Universitaet Muenster, 2017.

[24] *Understanding Photomultipliers, 1st Edition (2011)*. ET Enterprises Ltd.

[25] Hamamatsu Photonics K.K. *Photomultiplier Tubes Basics and Applications, 3rd Edition*. Hamamatsu Photonics K.K., 2007.

[26] A. G. Wright. *The Photomultiplier Handbook*. Oxford University, 2017.

[27] E. H. Bellamy et al. Absolute calibration and monitoring of a spectrometric channel using a photomultiplier. *NASA STI/Recon Technical Report N 95 (1993) 24635*, 1993.

[28] R. Bruijn and D. van Eijk. The km3net multi-pmt digital optical module. *Proceedings of Sience*, 2015.

[29] Marc Tippmann. Bremsstrahlung andfluorescencein photomultiplierscausingfast afterpulses. Technical report, 2013.

[30] Y. Abe at all. Characterization of the spontaneous light emission of the PMTs used in the double chooz experiment. *Journal of Instrumentation*, 11(08):P08001–P08001, aug 2016.

[31] S. Adrián-Martínez at al. A method to stabilise the performance of negatively fed km3net photomultipliers. *Journal of Instrumentation*, 11(12):P12014–P12014, dec 2016.

[32] Andor technology digital camera fundamentals.

[33] *Newton CCD Manual*.

[34] Markus Dittmer. Charakterisierung von photomultipliern mit hoher quanteneffizienz vom typ hamamatsu r12199 hqe. Master's thesis, WWU Muenster, 2017.

Danksagung

Ich danke Raffi dafür, dass sie mir ihren fancy Platz überlassen hat, mal wieder. :D

Ich danke Martin für seine aufopferungsvolle Hilfe bei eigentlich allem.

Ich danke meinen Eltern für ihre Unterstützung in allen Lebenslagen.

Ich danke jedem aus der Arbeitsgruppe dafür, dass sie die beste überhaupt ist.

Ich danke Daniel einfach mal random.

Ich danke Cirs für die aufrecht Erhaltung der Donnerstags Tradition.

Ich danke Alexander für die Aufnahme in diese tolle Arbeitsgruppe.

Natürlich danke ich auch Lew für seine fröhliche Art, seinen lustigen Geschienten

Ich danke Leuten von der IceCube Kollaboration, die alle so nett sind.

Ich danke denn Münster Marauders.

Und ich danke der Familie für viele tolle Stunden.

Declaration of Academic Integrity

I hereby confirm that this thesis "**Investigations of background light sources in photomultiplier tubes operated at negative high voltage**" is solely my own work and that I have used no sources or aids other than the ones stated. All passages in my thesis for which other sources, including electronic media, have been used, be it direct quotes or content references, have been acknowledged as such and the sources cited. I agree to have my thesis checked in order to rule out potential similarities with other works and to have my thesis stored in a database for this purpose.
